

Understanding the mechanism of SAAP-148 and exploring the purification of LptD/E

Major Research Project Report
NMR Spectroscopy Group
2021-2022

Dave Matser
6215165

Daily supervisor:
Rhythm Shukla

Examiner:
Dr. Markus Weingarth

Second reviewer:
Dr. Eefjan Breuking



Utrecht University

Table of contents:

Abbreviations	3
Chapter 1	4
SAAP-148	4
Abstract	5
Layman’s abstract.....	6
Introduction.....	7
Escape mechanisms.....	7
Antimicrobial peptides	8
LL-37	9
SAAP-148	10
Study objective	11
Materials and methods	12
Materials.....	12
Preparation of large unilamellar vesicles (LUVs).....	12
Static ³¹ P ssNMR	12
Isothermal titration calorimetry (ITC)	12
Magic angle spinning ³¹ P ssNMR	12
Carboxyfluorescein Leakage Assays	13
Results	14
Screening the effect of SAAP-148 on membrane lipids using ssNMR.....	14
The binding affinity of SAAP-148 with membrane lipids using ITC	15
Leakage assays performed with different membrane compositions.....	18
Discussion	20
Chapter 2	23
LptD/E.....	23
Abstract	24
Introduction.....	25
Cell envelope of Gram-negative bacteria.....	25
The LPS transport chain with LptD/E.....	26
Murepavadin	27
Study objective	28
Materials and methods	29
Materials.....	29
Transformation of LptD/E _{his}	29
	1

Expression of LptD/E _{his}	29
Purification of LptD/E _{his}	29
Results and Discussion	31
Transformation of vectors containing LptD and LptE in BL21 cells.....	31
Expression of LptD/E	32
Purification of the LptD/E complex	32
Acknowledgments	34
Literature.....	Error! Bookmark not defined.
Supplementary Data.....	35

Abbreviations

AMR	antimicrobial resistance
MDR	multidrug resistance
AMP	antimicrobial peptides
CL	cardiolipin
CAMP	cathelicidins antimicrobial peptides
PBS	phosphate-buffered saline
MAS	magic angle spinning
ssNMR	solid-state nuclear magnetic resonance
ITC	isothermal titration calorimetry
LUVs	unilamellar vesicles
DO(PG)	1,2-Dioleoylphosphatidylglycerol
DO(PE)	1,2-dioleoyl-sn-glycero-3-phosphoethanolamine
DO(PC)	1,2-dioleoyl-sn-glycero-3- phosphocholine
SQDG	sulfoquinovosyl diacylglycerols
CF	carboxyfluorescein
SAAP	synthetic antimicrobial and anti-biofilm peptides
LPS	lipopolysaccharide
MDR	multidrug resistance
WHO	World Health Organisation
IM	inner membrane
OM	outer membrane
<i>Pa</i>	<i>Pseudomonas aeruginosa</i>

Chapter 1

SAAP-148

Abstract

In the race against antimicrobial resistance, De Breij *et al.* (2018) designed an antibiotic peptide called SAAP-148 derived from the amino acid sequence of the human antimicrobial peptide LL-37. SAAP-148 showed to have high efficacy not only against multidrug-resistant ESKAPE pathogens but also against biofilms and persister cells. Yet, the exact binding mechanism of SAAP-148 is unknown. In this study, we use ssNMR and binding studies to show that the affinity of SAAP-148 is aspecific and it binds to all anionic lipids. Additionally, we use carboxyfluorescein leakage assays to study the effect of SAAP-148 on the permeabilization of the lipid vesicles. This data unexpectedly shows that the permeabilization of SAAP-148 is not coherent with the affinity of the negative charge of the lipids. SAAP-148 permeabilizes not only DOPG but DOPC membranes as well. On the other hand, SAAP-148 has only small a perturbation effect on the anionic lipid, cardiolipin. This information can be used to improve the antimicrobial properties of SAAP-148 and in the design of better antibiotics.

Layman's abstract

Some bacteria can cause serious infections that can be fatal. Therefore, research has focused on the development of antibiotics that can kill bacteria and cure infections. Unfortunately, due to excessive use of those antibiotics in, for example, the agriculture and health sector, bacteria developed mechanisms to become resistant to antibiotics. Now we are in desperate need of new drugs that resistant bacteria cannot escape. One way to design new antibiotics is to mimic naturally occurring human defense molecules, called peptides. One such peptide that we can use as a template is called LL-37. The research group of De Breij *et al.* developed a peptide that is like LL-37 but shows better antibiotic properties. This peptide is called SAAP-148. SAAP-148 has shown to be effective against bacteria, but how it works is yet unknown. Therefore, in this study, we aim to understand the binding mechanism of SAAP-148 to different membranes of bacteria, mammals, and plants. The difference between those membranes is mostly the net charge. SAAP-148 itself is positively charged. We use methods that can analyze the strength of the interaction between SAAP-148 and the membranes. Furthermore, we want to see the effect of SAAP-148 on the membranes. We use a method to see if the membranes get leaky when treated with SAAP-148. Our results show that SAAP-148 preferably interacts with the negatively charged membranes. But the leakiness of the membranes is affected by something else as well. SAAP-148 seems to have a leaky effect on both neutral and negatively charged membranes. More research is necessary to understand this exact binding mechanism so that the antimicrobial properties of the drug can be improved.

Introduction

The world is facing a silent pandemic caused by bacteria becoming increasingly resistant to antibiotics. The primary cause of this resistance is the worldwide and excessive use of antibiotics in, for example, the architecture and medical sectors (Ventola, 2015). The increase in this antimicrobial resistance (AMR) in Gram-positive but especially Gram-negative bacteria is causing major fatal infections (Willyard, 2017). Most of these infections occur in hospitals and result in the death of many patients (De Brij *et al.*, 2018). In 2019, an estimate of 1.27 million deaths was associated with bacterial AMR and this number could rise to annually 10 million deaths by the year 2050 (Murray *et al.*, 2022).

Escape mechanisms

A group of nosocomial pathogens that are often multidrug-resistant (MDR) and cause life-threatening infections are the so-called ESKAPE pathogens (*Enterococcus faecium*, *Staphylococcus aureus*, *Klebsiella pneumoniae*, *Acinetobacter baumannii*, *Pseudomonas aeruginosa*, and *Enterobacter*). Except for *Staphylococcus aureus*, all these species are Gram-negative. These pathogens have developed defense mechanisms to “escape” the mechanisms of current antibiotics (figure 1) (Rice, 2018).

One of the defense mechanisms of these bacteria is the composition of their cell envelope. This shields the bacterium from harsh environments and influx-efflux of molecules, making the transport of antibiotics across the membrane challenging (Botos *et al.*, 20216). The

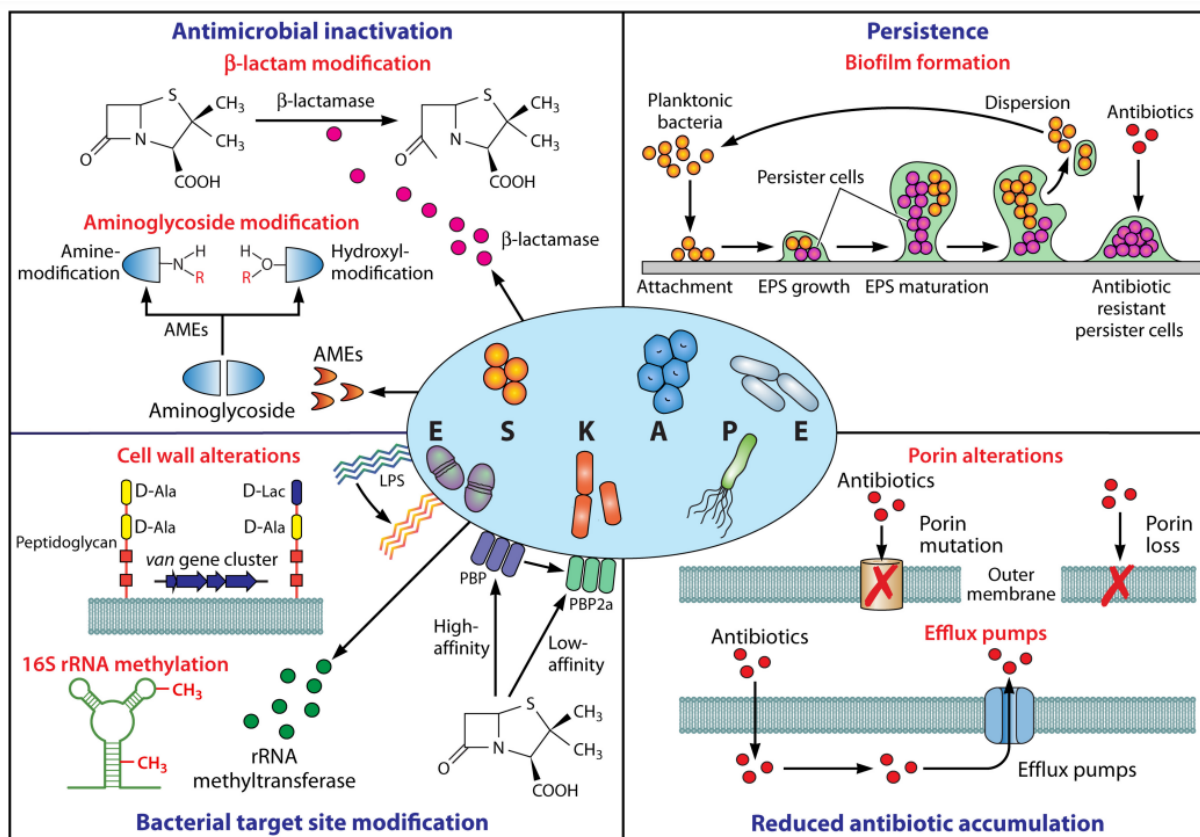


Figure 1. Visualization and examples of four groups of mediators of antimicrobial resistance in ESKAPE pathogens. (1) Enzyme-mediated antimicrobial inactivation. (2) Persister cells and biofilm formation causes high tolerance to antibiotics. (3) Bacterial target site modification, prevents the binding and reduces the affinity of

the antibiotic. (4) Less accumulation of antibiotics by the expression of efflux systems. AMEs, aminoglycoside-modifying enzymes; LPS, lipopolysaccharide; PBP, penicillin-binding protein; EPS, extracellular polymeric substance (Illustration adapted from De Oliveira *et al.*, 2020).

bacteria can adapt to the antibiotics by making alterations in the cell wall and porin compositions (De Oliveira *et al.*, 2020). Another ability of the ESKAPE species is to form biofilms; a self-produced matrix of extracellular substances with aggregates of bacteria to encase bacterial cells (Flemming and Wingender, 2010). Since this biofilm acts as a barrier, it can cause bacteria to be 100 to 1000 times more tolerant to antibiotics (Olsen, 2015). Furthermore, some bacteria in a colony can become persister cells that are in a dormant state and are highly tolerant to antibiotics (De Breij *et al.*, 2018). The reduced growth rate makes them less sensitive, which can make them outlast an antibiotic treatment and afterward repopulate the site (Olsen, 2015). Development of new antibiotics that can tackle, not only growing bacteria but also these biofilms and persister cells is therefore desperately needed.

Antimicrobial peptides

Naturally occurring mammalian antimicrobial peptides (AMPs) can serve as a promising template for a new generation of antibiotics. AMPs are small cationic, amphipathic peptides that can kill bacteria with surprisingly diverse mechanisms of action. They mostly kill bacteria by disrupting and permeabilizing their membranes, but also inhibit protein and DNA synthesis and can repress cellular processes like protein folding. This broad range of action makes them less sensitive to AMR (Aoki & Ueda, 2013). AMPs are expressed in cell types that are likely to encounter pathogens, like epithelial cells or airway surfaces but are also expressed in innate immune cells like monocytes and macrophages. (Burton & Steel, 2009).

The key reason why AMPs are bacterial specific is due to the different composition of lipids in the bacterial and mammalian cytoplasmic membranes. Mammalian membranes bear no net charge and are mainly composed of the zwitterionic phosphatidylcholine (PC) lipid. Bacterial membranes, on the other hand, are composed of lipids such as the cationic phosphatidylethanolamine (PE), but predominantly the anionic lipids like phosphatidylglycerol (PG) and double negatively charged cardiolipin (fig. 2). Overall, the bacterial membrane is more negatively charged than mammalian membranes. Since the AMPs are positively charged, they can act on this difference by interacting preferentially with the negatively charged membranes and only less, or not at all with the mammalian membranes (Sevcsik *et al.*, 2008). Furthermore, binding is established by the hydrophobic interactions between the amphipathic domain of the peptide and the phospholipid membrane (Holleman *et al.*, 2018).

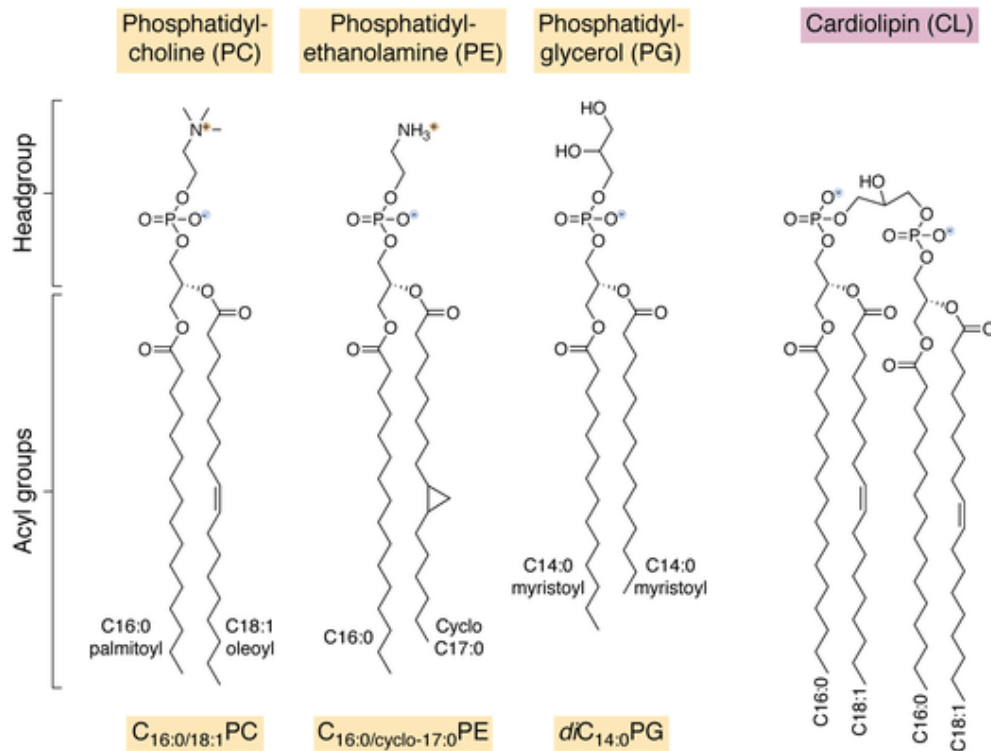


Figure 2. Schematic visualization of common phospholipids. Schematic visualization of the common phospholipids found in mammalian and bacterial outer membranes (Illustration adapted from Horne *et al.*, 2022).

LL-37

Human AMPs are divided into two big classes: defensins and cathelicidins (CAMPs). The main difference between the two classes is that defensins contain a β -sheet whereas CAMPs have an α -helix (Verjans *et al.*, 2016). Although there are more than a hundred human AMPs identified, there is only one human CAMP known (Verjans *et al.*, 2016). This is called LL-37 and it has been studied in depth (fig. 3A & B). The LL-37 peptide exerts a broad range of antimicrobial activities by non-specifically disrupting the microbial membranes, neutralizing antimicrobial endotoxins, and interrupting biofilms. (Riool *et al.*, 2018). Moreover, LL-37 acts as a modulator of the immune system by guiding cells to the site of infection and binding to at least nine receptors. All these mechanisms make it difficult for bacteria to develop resistance to LL-37 (Burton & Steel, 2009).

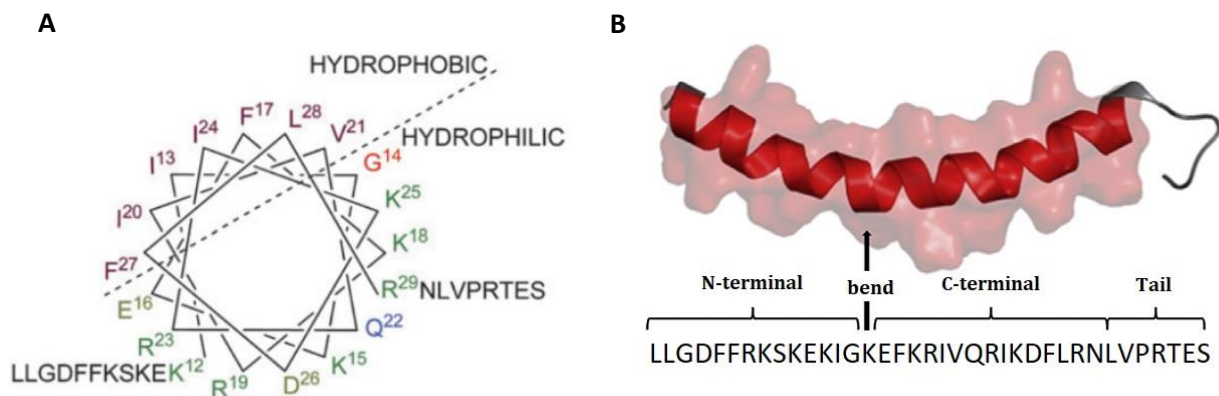


Figure 3. Schematic visualization LL-37 (A) Helical wheel diagram of LL-37 showing the N- and C-terminal residues as unstructured and the 12-29 residues as an amphipathic helix. (B) A three-dimensional α -helical structure of LL-37 with its sequence (Illustrations adapted from Burton & Steel, 2009 and Vandamme *et al.*, 2012).

Despite their great potential, AMPs still have unfavorable properties, for example, high production cost, instability in human plasma, deactivation by high salt concentrations, and toxic hemolytic activity. Furthermore, AMPs like LL-37, have a broad spectrum of activity that could lead them to interact with host cells and disrupt the indigenous microflora of the human body (Aoki & Ueda, 2013). LL-37, for example, has been shown to have an LC_{99.9}, which is the lowest peptide concentration that would result in >99.9% of *S. aureus*, of only 1.6-6.4 μ M in phosphate-buffered saline (PBS), but more than 204,8 μ M in 50% human plasma. This shows that LL-37 is less active in human plasma (De Breij *et al.*, 2018). To improve these properties, research needs to be done on the exact working mechanism of these AMPs. Furthermore, novel AMPs can be designed with improved biochemical properties (Aoki & Ueda, 2013).

SAAP-148

Due to the exceptional antimicrobial activity of LL-37, many research groups are trying to develop synthetic peptides that have similar activity as LL-37 but have improved antibiotic properties. De Breij *et al.* (2018) from Leiden University recently developed a set of LL-37 inspired synthetic antimicrobial and anti-biofilm peptides also known as SAAPs. The focus of this design was to keep the α -helical structure intact (fig. 3B) and to increase the hydrophobicity of the molecule. They also increased the net cationic charge by exchanging the glutamine (Q) residues present in LL-37 with arginine (R) or lysine (K) (fig. 4). The peptides were designed with the use of deep learning computer models.

Peptide:	Sequence:	Net charge:
LL-37	LLGDFFRKSKEKIGKE F KRI VQRI KDF L RNLVPRTE S	+ 6
SAAP -148	LKR VWKRVFKL LKRYWRQLKKPVR	+ 11

Figure 4. aligned sequences of LL-37 and SAAP-148. The amino acid sequences of LL-37 and its derived peptide SAAP-148 were compared. The net charge of the peptides is given as well.

After the design, the peptides were tested for their activity against *S. aureus* and *P. aeruginosa* in buffer and 50% human plasma. One of these peptides, called SAAP-148, was the most promising that demonstrated efficacy not only against MDR pathogens of the ESKAPE species but also against biofilms and persister cells. Compared to LL-37, lower concentrations of SAAP-148 were needed to reach >99.9% killing of *S. aureus* in both buffer and plasma.

Furthermore, De Breij *et al.* used methods like differential scanning calorimetry (DSC) and fluorochrome leakage analyses of bacterial membranes to assess whether SAAP-148 works in a similar fashion as LL-37 by permeabilizing the membrane. They found that SAAP-148 first perturbed the hydrophobic core of the lipid bilayer which resulted in thinning of the membrane. SAAP-148 permeabilizes the membrane of *S. aureus* and *A. baumannii* in a time and dose-dependent matter, leading to the death of the bacteria in minutes (fig. 5). Moreover, single-dose and 14-day repeated-dose dermal toxicity studies were performed to assess the

safety of SAAP-148 as an ointment. The results showed no signs of skin irritation or pathology (De Breij *et al.*, 2018).

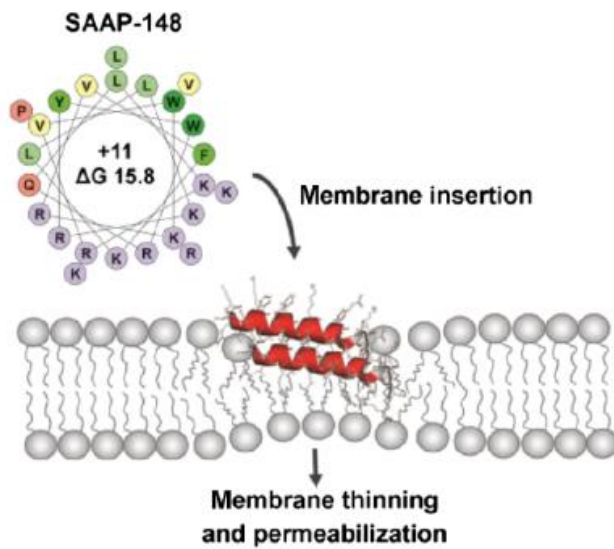


Figure 5. Schematic visualization of the interaction of SAAP-148 with the bacterial membrane. A helical wheel diagram of SAAP-148 with the charged amino acids in purple. The net charge and hydrophobicity are shown in the middle of the wheel. The α -helical structure of the peptide is visualized in the membrane (Illustration adapted from De Breij *et al.*, 2018).

Study objective

While it was reported that SAAP-148 works by membrane thinning and permeabilization of the membrane (De Breij *et al.*, 2018), the exact binding mechanism is yet unknown. Here, we used static and magic angle spinning (MAS) ^{31}P solid-state nuclear magnetic resonance (ssNMR) and isothermal titration calorimetry (ITC) to evaluate the interaction of SAAP-148 with lipid membranes of different compositions. We used artificial membranes in the form of large unilamellar vesicles (LUVs) with different lipid compositions that mimic mammalian or bacterial membranes, to investigate how this peptide interacts with lipid membranes. We focus on the zwitterionic mammalian lipid 1,2-dioleoyl-sn-glycero-3-phosphocholine (DOPC) and on the bacterial lipids such as anionic 1,2-Dioleoylphosphatidylglycerol (DOPG), anionic cardiolipin, and zwitterionic 1,2-dioleoyl-sn-glycero-3-phosphoethanolamine (DOPE). Furthermore, we also look at Sulfoquinovosyl diacylglycerols (SQDG), a negatively charged lipid found in plants, to see if SAAP-148 binding is specific to the structure of the membrane or if an anionic charge suffices. After this, we studied the permeabilization effect of SAAP-148 on different LUVs with a leakage assay.

Materials and methods

Materials

SAAP-148 was obtained from Dr. P.H. Nibbering from LUMC.

The phospholipids 1,2-dioleoyl-sn-glycero-3-phosphocholine (C18:1, DOPC), 1,2-dioleoyl-sn-glycero-3-phosphoglycerol (C18:1, DOPG), 1,2-dioleoyl-sn-glycero-3-phosphoethanolamine (C18:1, DOPE), 1',3'-bis[1,2-dioleoyl-sn-glycero-3-phospho]-glycerol (C18:1, Cardiolipin) and sulfoquinovosyldiacylglycerol (SQDG) were purchased from Avanti Polar Lipids, Inc. (fig. 6).

Preparation of large unilamellar vesicles (LUVs)

Lipid stocks were made by dissolving the desired lipids in chloroform and stocks were saved at -20°C. The exact concentration of PO₄⁻ in the lipid stocks was determined by the Rousers method (Rouser, Fleischer & Yamamoto, 1970). An appropriate amount of phospholipid from these stocks was used to make lipid films in a vial glass wall by evaporating under a nitrogen stream. The lipid film was resuspended in 500 µl of buffer (20 mM Tris, 25 mM NaCl, pH 7.4) by vortexing at room temperature. LUVs were made by extrusion (Whatman Nucleopore, Track-Etch Membranes), using 21 passes through a two stacked 0.2 µm or 0.4 µm polycarbonate filter at room temperature. The exact concentration of PO₄⁻ in the vesicles was again determined by the Rousers method.

Static ³¹P ssNMR

The 0.4 µm LUVs, prepared as mentioned above, with 5000 nmols of lipids DOPG and DOPC with and without SAAP-148 were spun down for 45 minutes at 60,000 X g at 4 °C. The samples containing SAAP-148 were incubated for 3 hours at 4 °C. The obtained pellet was transferred to a 3.2 mm rotor. The spectra were obtained using a 500 MHz Bruker spectrometer. The experiment was run for 24 hours.

Isothermal titration calorimetry (ITC)

For the ITC experiments, lipid vesicles were prepared, consisting of 6.4 mM DOPG, 7.4 mM DOPC, 3.5 mM DOPC/E (containing 50 mol% DOPC and 50 mol% DOPE), 7.0 mM cardiolipin (containing 50 mol% cardiolipin and 50 mol% DOPC) and 1.7 mM SQDG (containing 50 mol% SQDG and 50 mol% DOPC). The ITC experiments were performed at 37°C using an Affinity ITC microcalorimeter (Walters LLC) with a 177 µl sample cell and 250 µl titration syringe. Samples were degassed under a vacuum for 10 minutes at 37 °C before an experiment. For each measurement, 2 µl of lipid vesicles were titrated into the sample cell containing 60 µM SAAP-148 in the same buffer (20 mM Tris, 25 mM NaCl, pH 7,4). The first injection had a volume of 0.5 µl. The interval between injections was 200-250 s. ITC data were analyzed with Nano Analyzer Software (Walters LLC) using the "independent" model. The baseline was corrected manually. Measurements were done in duplicates or triplicates.

Magic angle spinning ³¹P ssNMR

The sample was prepared as mentioned above. The spectra were obtained using a 500 MHz Bruker spectrometer. The sample was spun at 10 kHz MAS at 260 K for 16 hours.

Carboxyfluorescein Leakage Assays

Lipid films were made containing 5000 nmols of DOPG, DOPC, and DOPC/cardiolipin (50 mol% DOPC and 50 mol% cardiolipin) and were dissolved in 1 ml of 50 mM of carboxyfluorescein (CF) (pH 7.5). The suspension was vortexed for 1 minute, let to rest for 5 minutes, and vortexed again for 1 minute. The lipid suspension was frozen in a CO₂/ethanol bath and thawed in a 37 °C bath 10 times. 200 nm LUVs were made by extrusion using 11 passes through the membrane. To get rid of the uncaptured fluorescence dye, we did the following steps: a Teflon disc was placed on the bottom of a 2.5 mL syringe and Sephadex G50 was added to fill the entire syringe. The syringe was placed in a glass tube and centrifuged at 3000 rpm for 2 minutes. The eluent was discarded. A new Eppendorf tube was placed in the glass tube under the syringe. The vesicle suspension was brought on top in the middle of the column. The vesicles were eluted by centrifugation at 3000 rpm for 2 minutes. The exact concentration of PO₄⁻ in the vesicles was determined by the Rousers method (Rouser, Fleischer & Yamamoto, 1970). The measurements were done on a fluorimeter and the fluorescence emission was recorded as a function of time. CF was irradiated at 492 nm and the detection was done at 515 nm. The cuvette was filled with 1 mL of buffer (10 mM Tris, 50 mM NaCl, pH 7.5) and 4 µl of vesicles were added. The baseline was determined for about 30 seconds. Then SAAP-148 was added to measure a range of concentrations from 0.0125 µM-20 µM. At about 2 min 1% Triton-X-100 was added as a positive control.

Results

Screening the effect of SAAP-148 on membrane lipids using ssNMR

First, we used static ^{31}P ssNMR to study the effect of SAAP-148 on mammalian zwitterionic DOPC and bacterial anionic DOPG LUVs. The LUVs were incubated with SAAP-148 peptide for 3 hours. As a control, both membranes were measured without SAAP-148.

As seen in the overlaid spectra (fig. 6A & B), the incubation of vesicles with SAAP-148 causes membrane perturbation. The result shows that this effect is greater for DOPG vesicles as compared to the zwitterionic vesicles.

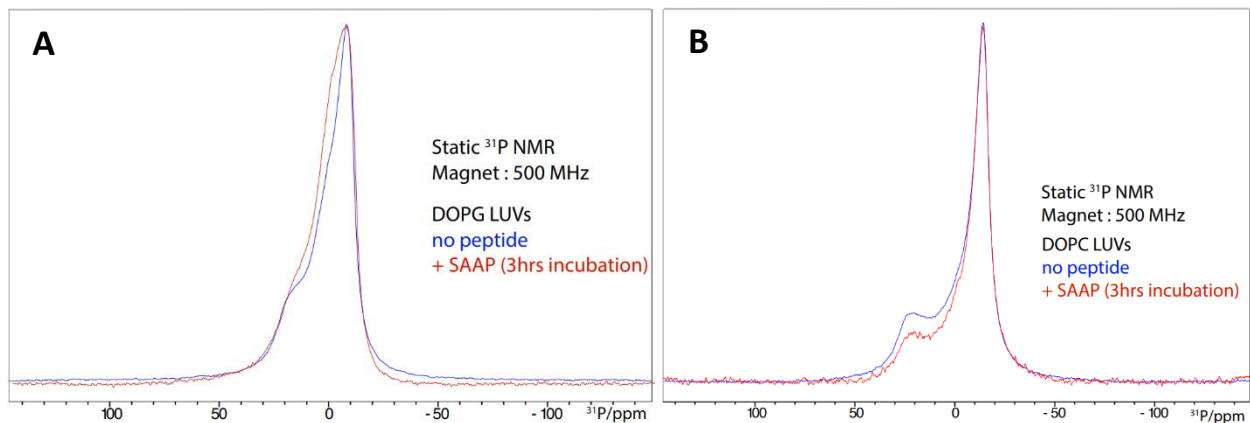


Figure 6. Static ^{31}P ssNMR spectra at 500 MHz of (A) DOPC LUVs and (B) DOPG LUVs with (red) and without (blue) SAAP-148. SAAP was incubated for 3 hours. The measurements were done overnight.

Since there is a bigger perturbation of the DOPG vesicles, we wanted to investigate this more. Therefore, we used MAS ^{31}P ssNMR to see if there is any change in the chemical shift of the DOPG lipids, as that would indicate a specific binding of SAAP-148 to the membrane. The obtained spectra (fig. 7) show two identical peaks of DOPG with and without SAAP-148. This demonstrates no specific binding of SAAP-148 to DOPG.

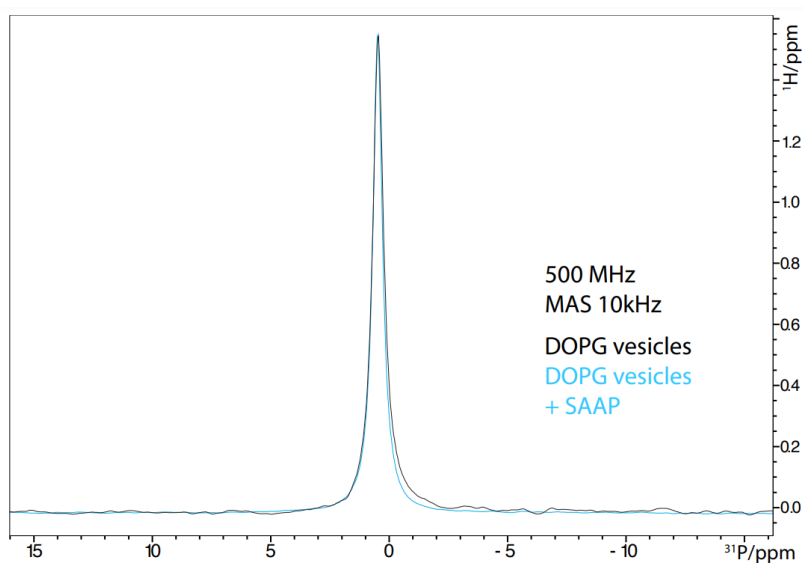


Figure 7. MAS ^{31}P ssNMR spectra of DOPG with and without SAAP-148. 10 kHz MAS at 260K for 16h (with SAAP) and 1h (without SAAP) at the 500 MHz Bunker spectrometer. Black represents DOPG vesicles without the addition of SAAP-148. Blue represents DOPG vesicles with 2,5 h incubation of SAAP-148.

The binding affinity of SAAP-148 with membrane lipids using ITC

The ssNMR data indicates that SAAP-148 perturbs the anionic membranes strongly as compared to the neutral DOPC vesicles. Therefore, we investigated this further by studying the binding affinity of SAAP-148 to different membranes with different charges. We did this with the use of Isothermal Titration Calorimetry (ITC). For all experiments, a buffer titration was performed as a background (supplemented figure S1) which shows that there is no considerable background interaction.

Firstly, we measured the binding affinity of SAAP-148 with the bacterial anionic LUVs of DOPG and cardiolipin. Since cardiolipin has a double negative charge, we made vesicles with a 1:1 ratio of cardiolipin and DOPC. This would give the LUVs the same net charge as DOPG vesicles. As can be seen in figures 8A and 8B, the reaction that occurred with both vesicles was exothermal and the heat release of the first few injections was high and gets saturated over time. This corresponds to the sigmoid binding curve in the lower panel and the low dissociation constant (K_D) of DOPG and cardiolipin of respectively $4.40E-06$ M and $2.46E-05$ M. The results indicate that SAAP-148 is not specific for DOPG but also binds strongly to other bacterial anionic lipids.


To check if SAAP-148 only binds to bacterial anionic lipids or is nonspecific and binds to more negatively charged cells, we used an anionic plant lipid called SQDG. We observed another strong interaction with a K_D of $3.63E-06$ M (fig. 8C). SAAP-148, therefore, is unspecific and binds to any anionic lipids. Furthermore, it seems that SAAP-148 has a higher affinity (10 fold higher) for single negatively charged lipids, compared to double negatively charged lipids.

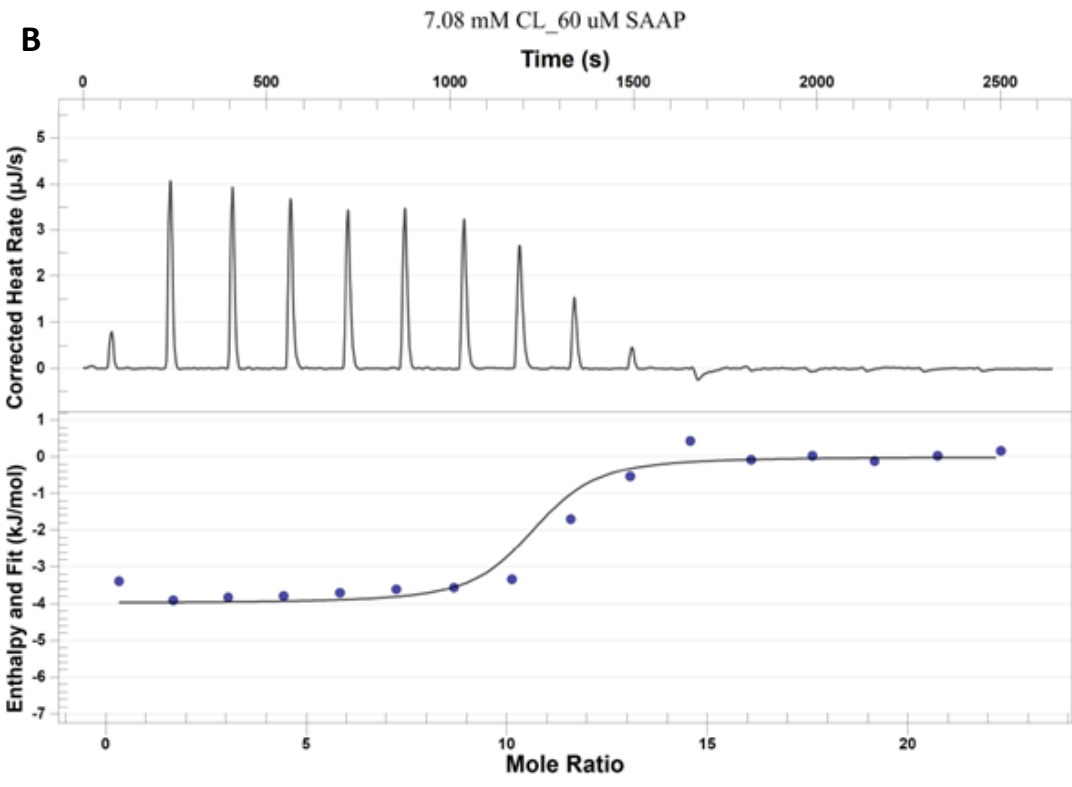
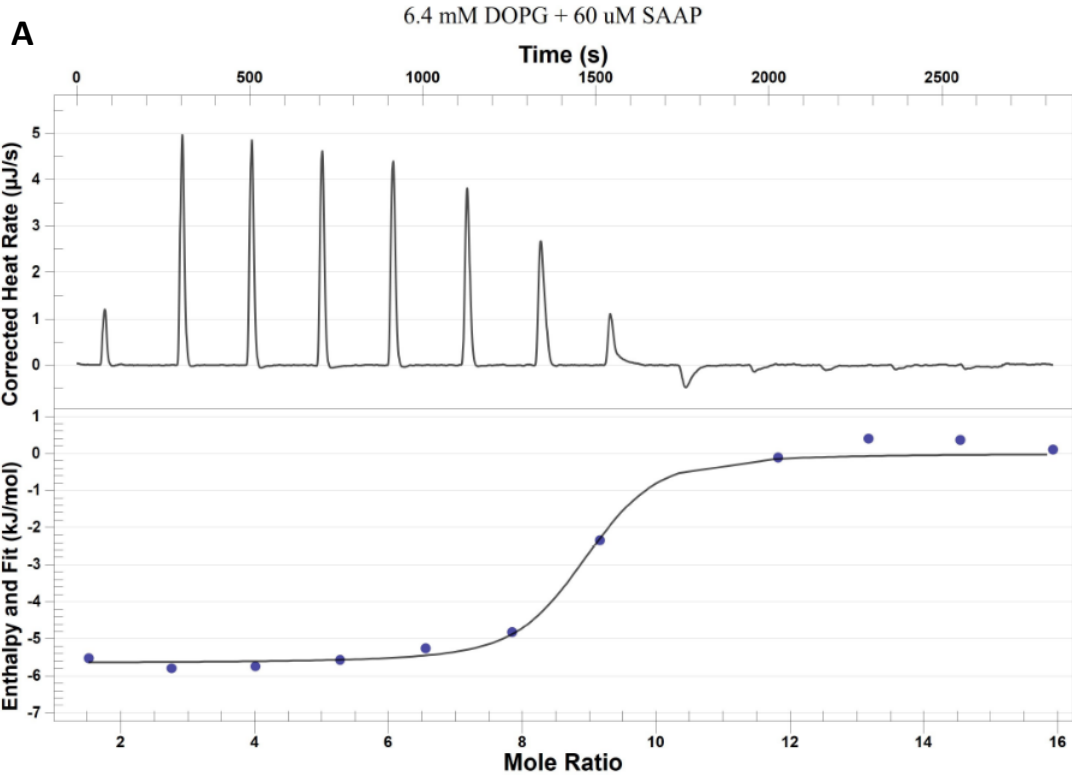
We repeated the experiments with zwitterionic LUVs of mammalian DOPC and bacterial DOPE lipids, to see if the binding affinity would be reduced. Both DOPC and DOPE showed similar binding curves (fig. 8D & S3A). A zoomed-in version of the thermograms can be found in the supplements (fig. S2 & S3B). Again, an exothermic reaction occurred, but this time with very low heat releases. The mean K_D value of both experiments was $1.00E-03$, which is the upper limit for our machine indicating a weak binding. Furthermore, there is no sigmoid binding curve observable. This data shows that SAAP-148 has very weak binding to zwitterionic LUVs.

Overall, SAAP-148 shows to have a higher affinity for anionic (Table 1). Furthermore, SAAP-148 binds to all negatively charged membranes and is therefore not bacterial specific. Since the reaction is mainly based on charge and there seems to be no specific binding, it can be described as an electrostatic interaction rather than a hydrogen bond formation.

Table 1. Dissociation constant (K_D) of SAAP-148 with various membrane lipids.

Lipid	K_D value (M) + SD
SQDG	$3.63E-06 \pm 3.72E-07$
DOPG	$4.40E-06 \pm 2.95E-06$
CL	$2.46E-05 \pm 1.02E-05$
DOPC	$1.00E-03$
DOPE	$1.00E-03$





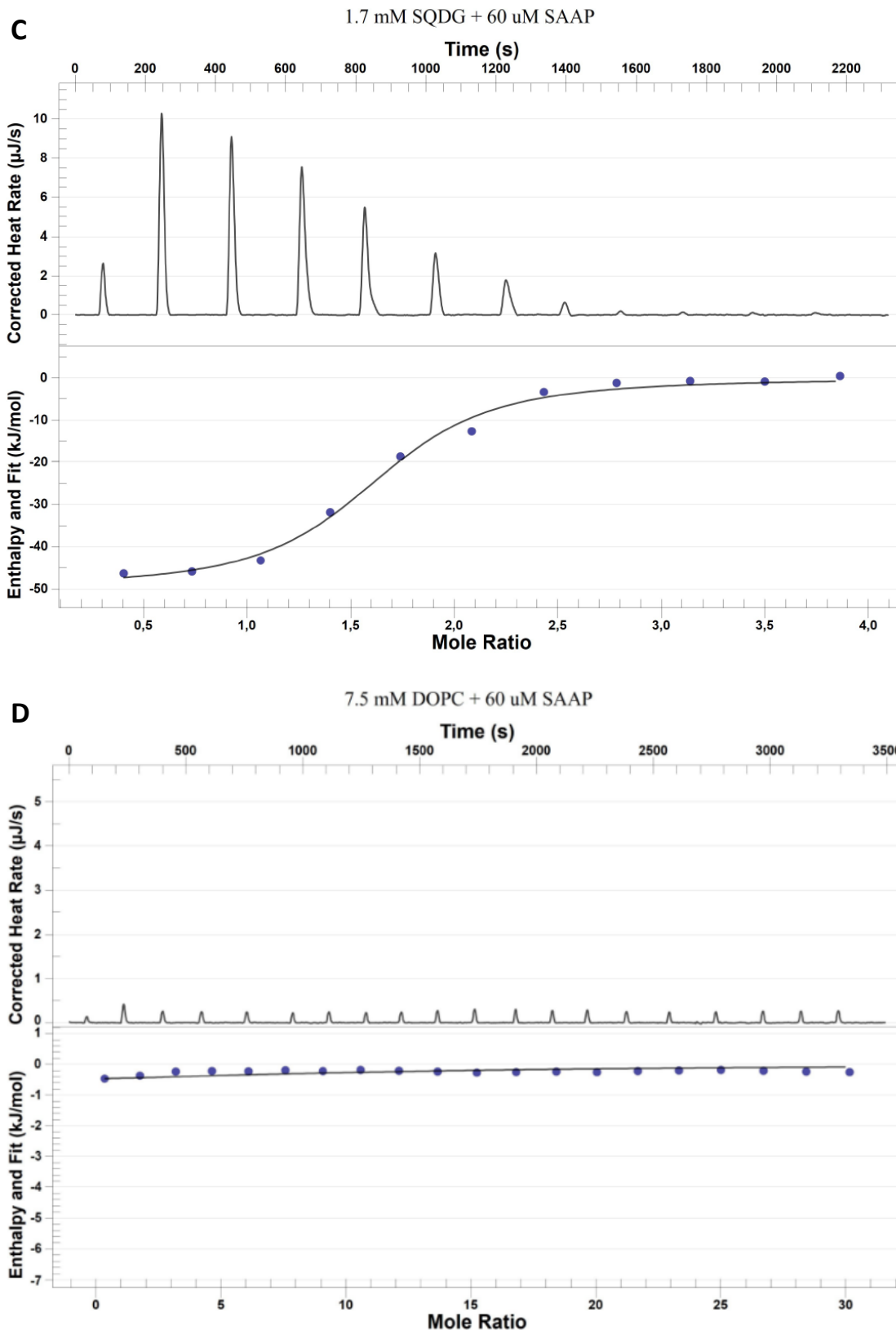


Figure 8. ITC thermograms of DOPG, CL, SQDG, and DOPC LUVs with SAAP-148. The top panel shows the corrected heat release whereby every peak corresponds with an injection. The line in the lower panel indicates the best fit with the independent model. The experiments were done in triplicates. Mean best fit K_D values with SD of (A) DOPG = $4.40\text{E-}06 \pm 2.95\text{E-}06$ M (B) CL = $2.46\text{E-}05 \pm 1.02\text{E-}05$ M (C) SQDG = $3.63\text{E-}06 \pm 3.72\text{E-}07$ M (D) DOPC = $1.00\text{E-}03 \pm 0$ M.

Leakage assays performed with different membrane compositions

Now we know that SAAP-148 preferably binds with the anionic lipids and, we were interested in its effect of it on the permeabilization of differently charged vesicles. The effect of SAAP-148 on disruption and permeabilization of the membrane of DOPG vesicles had been studied before (De Breij *et al.*, 2018). Thus using that as a starting point, we repeated this experiment, but with CF (fig. 9D) instead of ANTS/DPX fluorophore, and looked at the permeabilization effect on cardiolipin and DOPC LUVs.

For DOPG, our results were comparable with the results from De Breij *et al.*, in which a higher concentration of SAAP-148 led to maximum permeabilization. However, in their experiments, a concentration of 2 μM was already enough to reach 100% leakage. Instead, we needed twice as much to reach maximum leakage (fig. 9A). We compared this with the effect seen on cardiolipin vesicles. Interestingly, a concentration of 2 μM SAAP-148 was enough to cause 45% permeabilization but increasing the peptide concentrations to even 20 μM did not affect the membranes any further (fig. 9B). This shows that SAAP-148 has less permeabilization effect on cardiolipin vesicles as compared to DOPG.

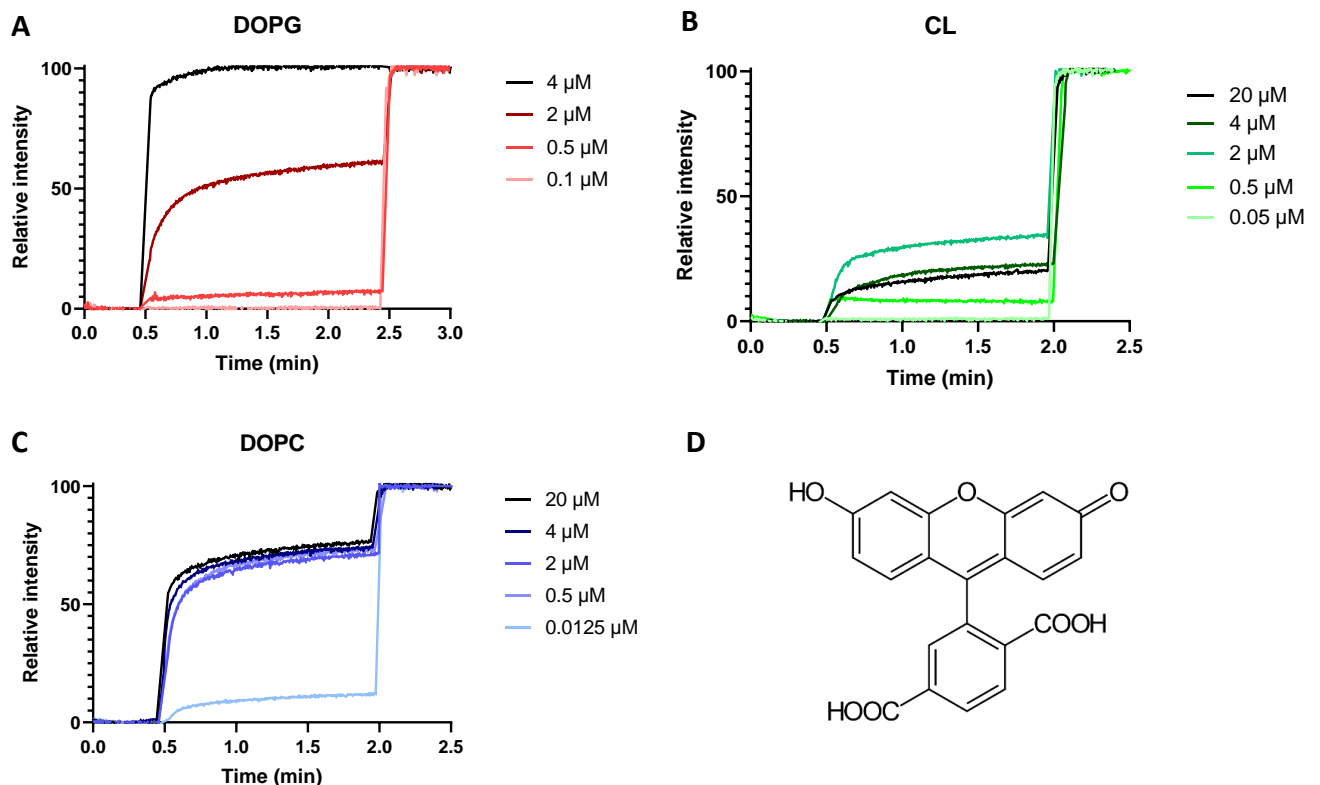


Figure 9. Carboxyfluorescein leakage measured for DOPG, DOPC, and CL LUVs in the presence of SAAP-148. A, B, C) Results are visualized as the relative intensity in function of time (minutes). The different colors represent the different concentrations of SAAP-148. At 30 seconds, SAAP-148 is added to the vesicles and at 2 minutes Tris-100-X is added to the vesicles. Measurements of different concentrations are performed in triplicates. (D) Visualization of Carboxyfluorescein chemical structure.

We also performed the same experiment for DOPC vesicles. Very low peptide concentrations (0.0125 μM) already disrupted the membrane. A concentration of 0.5 μM caused a maximum leakage of 75%. Higher concentrations did not result in further disruption of the cells (fig. 9C). This data implies that SAAP-148 does permeabilize DOPC membranes even though it binds very weakly to the membrane.

Discussion

De Breij *et al.* (2018), designed a synthetic antimicrobial and antibiofilm peptide called SAAP-148 that was based on the human antimicrobial peptide LL-37. SAAP-148 showed high efficacy against ESKAPE species, biofilms, and persister cells, which is supposed to relate to the interactions of the peptide with bacterial membranes. However, how the peptide interacts with bacterial membranes, and why it would be specific to bacteria is yet unknown. In this study, we investigated the membrane-binding mechanism of SAAP-148 and addressed the binding specificity of SAAP-148 to different membranes. Furthermore, we explored the effect of SAAP-148 on the permeabilization of different membranes.

With calorimetric studies, we studied the binding affinity of SAAP-148 with different membrane lipids. Our data shows that SAAP-148 has a high affinity for negatively charged lipids and barely interacts with neutral lipids. SAAP-148, therefore, showed to be aspecific and binds to different negatively charged membranes of both bacterial and plant lipids. This could be explained by the fact that SAAP-148 has a net positive charge of +11 and therefore shows immense electrostatic interactions with negatively charged membranes. Our MAS ssNMR data supports this theory of aspecific binding since we observed no bound state or changes in the chemical shift of the DOPG membranes upon the addition of SAAP-148.

Although there is no specific binding, just like other AMPs, SAAP-148 preferably interacts with the negatively charged membranes. Since most mammalian membranes are composed of neutral lipids like DOPC, SAAP-148 should not be toxic to them making it a suitable drug candidate.

Furthermore, we investigated the effect of SAAP-148 on the permeabilization of the different membranes. The leakage assays of DOPG have been performed previously by De Breij *et al.* (2018) and although we obtain similar results, we needed higher peptide concentrations to achieve 100% leakage. This could be explained by the difference in fluorescence markers used for these experiments. De Breij *et al.* used ANTS/DPX which is a small molecule that can leak out due to minimal perturbations at low concentrations of SAAP-148. Whereas carboxyfluorescein being bigger, required higher perturbations for the membranes to show a similar effect. This shows SAAP-148 perturbs the membranes of DOPG to cause leakage of ions, water, and other small molecules up to 380 Da in size.

We also performed similar experiments with Cardiolipin. However, these assays only showed very small amounts of leakage. This could be explained by the 10x lower affinity of SAAP-148 for cardiolipin compared to DOPG. Unfortunately, it is known that bacteria can adjust their lipid compositions by converting DOPG to cardiolipin under stressful conditions. Thus, this can be used as a resistance mechanism by bacteria to escape SAAP-148.

On the contrary, the effect of SAAP-148 on DOPC membranes was unexpected. Although SAAP-148 has a very low affinity toward DOPC, the peptide already disrupted the vesicles at very low concentrations. SAAP-148, therefore, seems to harm the DOPC membranes. The effect of SAAP-148 on DOPC, and therefore mammalian membranes, does make it questionable if SAAP-148 can function as a good antibiotic candidate. Nevertheless, the vesicles never reached 100% leakage and De Breij *et al.* have performed toxicity studies that demonstrated no toxic effect of SAAP-148 treatment on dermal cells. This poses an interesting scenario where although SAAP-148 shows negligible binding to DOPC, it still manages to

permeabilize the membranes heavily. It could be an interesting aspect to study how the mammalian cells, like the ones tested by De Breij *et al.* protect themselves from the permeabilization effects of SAAP-148. Such studies can provide insight into better formulations to administer SAAP-like peptides to reduce the toxicity even further.

To conclude, the SAAP-148 peptide seems to have a strong electrostatic interaction with anionic membranes. Although, both DOPG and cardiolipin are anionic bacterial lipids, SAAP-148 has a dose-dependent permeabilization effect on DOPG and minor effects on cardiolipin (fig. 10). Furthermore, SAAP-148 seems to have a permeabilization effect on mammalian DOPC lipids, which questions the toxicity of the peptide.

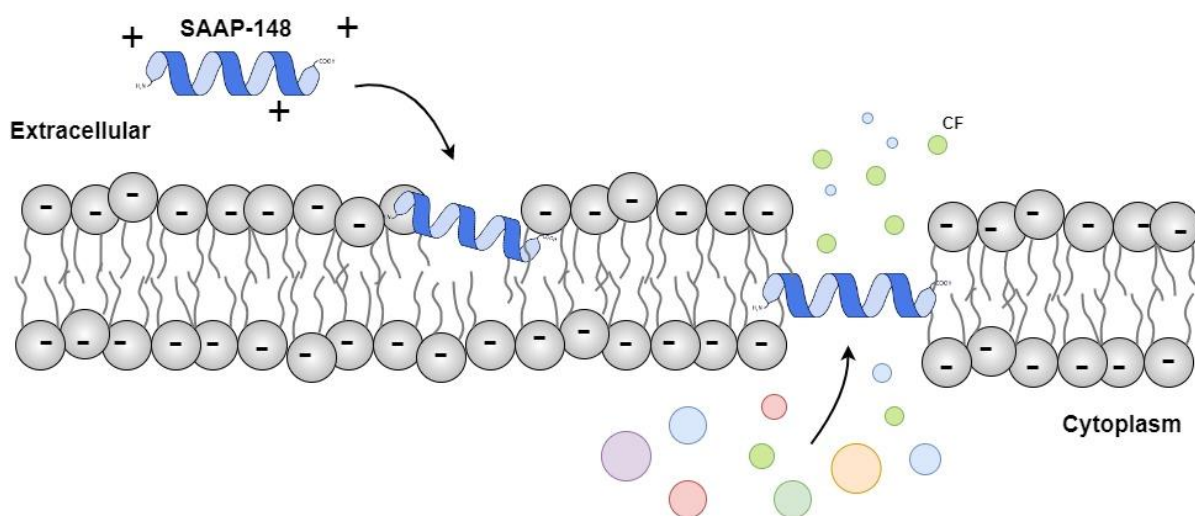


Figure 10. Schematic representation of the mode of action of SAAP-148. The positively charged SAAP-148 binds to the negatively charged membranes and permeabilizes it, causing leakage of small molecules like CF.

More research is needed to investigate the binding mechanism and interaction of SAAP-148 to different membranes in further detail. Further experiments could include other leakage assays with the use of membrane lipids like DOPE and SQDG or with live bacteria. Since the permeabilization effect of SAAP-148 can differ in human plasma compared to buffer, the leakage experiments should be repeated with 50% human plasma to map the differences. Moreover, the use of a bigger fluorescence dye can show the effect of permeabilization on leakage of larger molecules, like proteins.

Finally, next steps in this research can also include ssNMR studies with other formulations, the use of real bacterial membranes, and selectively isotopically labeled SAAP-148. Studies with isotopically labeled SAAP-148 can give more insight into understanding which part of the peptide is bound to the membrane. Similar experiments have been performed by Weingarh's group to study the mode of action of teixobactin (Shukla *et al.*, 2020). These experiments can give information about the structural changes in the peptide upon binding to the membrane, dynamics of the peptide in the bound state, and information on the orientation of the peptide on the surface of the membrane.

Information about the mechanism of SAAP-148 will help in the improvement of this antimicrobial properties. Furthermore, the knowledge of mechanisms of such peptides can help in the development of better synthetic antimicrobial and anti-biofilm peptides.

Chapter 2

LptD/E

Abstract

Gram-negative bacteria are more resistant to antibiotics as compared to Gram-positive bacteria. One of the reasons for this is the difference in their cell envelope structure. The outer membrane (OM) of Gram-negative bacteria contains a phospholipid inner leaflet and an almost entirely lipopolysaccharide (LPS) outer leaflet. LPS shields the bacteria from harsh environments and incorporation of LPS is essential for bacterial survival. LPS is incorporated into the membrane by the LPS-transport chain, facilitated by seven proteins (LptABCDEFG). The most accessible part of these proteins is the LptD/E complex. This complex is embedded in the outer membrane of the envelope and performs the final step of the transportation by incorporating the LPS in the outer membrane. An antibiotic, called Murepavadin, binds to this LptD/E complex in *Pseudomonas aeruginosa* (*Pa*) and inhibits the incorporation of LPS in the OM. In this study, we give insight into the transformation, expression, and purification of the *Pa* LptD/E complex that could be used in further studies to investigate the binding of Murepavadin to this complex using solid-state NMR.

Introduction

As described previously, the development of new antibiotics is desperately needed due to the rise in antibiotic multidrug resistance (MDR) (Rice, 2018). Most of the MDR pathogens are primarily Gram-negative bacteria. According to the World Health Organization (WHO, 2017), fifteen out of eighteen pathogens on their priority list are Gram-negative. Therefore, there is an urgent demand for the development of novel compounds that can tackle these types of bacteria. One of the main differences in characteristics between Gram-positive and Gram-negative bacteria is the cell envelope structure. Thus, researchers are trying to find a drug that can tackle parts of these specific cell envelope structures (Ruiz, Kahne, Silhavy, 2006).

Cell envelope of Gram-negative bacteria

The cell envelope of Gram-negative bacteria is composed of a symmetric inner membrane (IM) and an asymmetric outer membrane (OM), separated by the periplasm which contains a peptidoglycan layer (Ruiz, Kahne, Silhavy, 2006). The IM is a typical phospholipid bilayer, containing inner membrane proteins (De Oliveira *et al.*, 2020). The OM, on the other hand, contains a phospholipid inner leaflet and an almost entirely lipopolysaccharide (LPS) outer leaflet, shielding the bacteria against harsh environments (Moehle *et al.*, 2016). Furthermore, the OM contains a lot of proteins that conduct essential functions like the uptake of nutrients, the efflux of waste, and OM biogenesis. Most of these proteins have a β -barrel fold (Prajapati *et al.*, 2021). All these cell envelope components make transportation of antibiotics across the membrane challenging (fig. 11) (De Oliveira *et al.*, 2020).

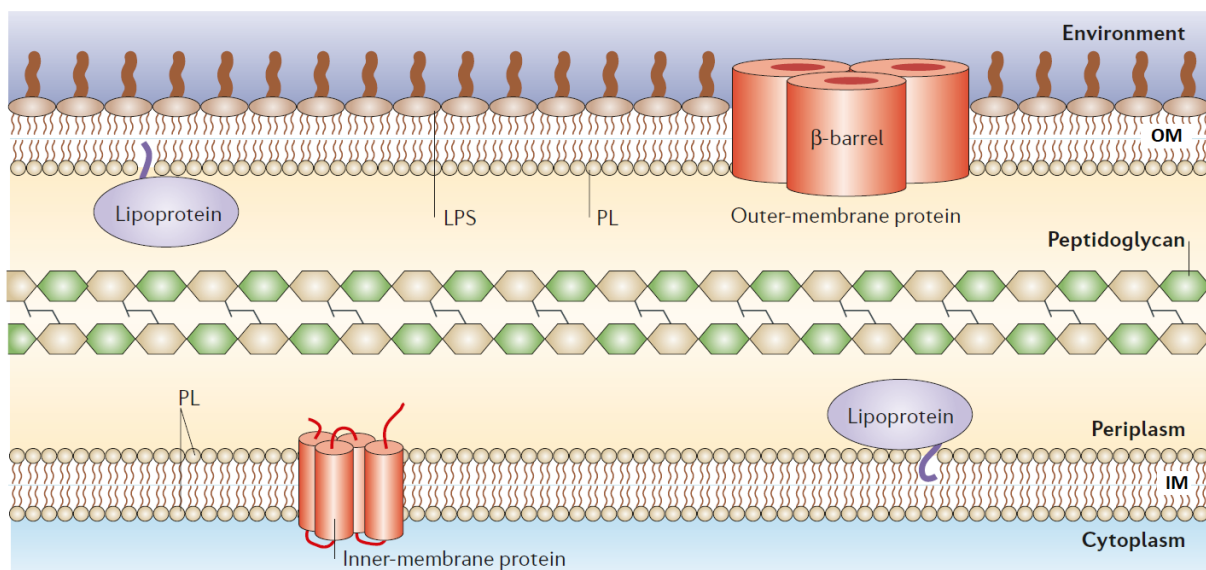


Figure 11. Visualization of the cell envelope structure of Gram-negative bacteria. Visualized is the Cytoplasm of a bacterium, surrounded by a cell envelope. The envelope is composed of the inner membrane (IM), the periplasm, and the outer membrane (OM). The IM is a symmetric bilayer composed of phospholipids (PL) that contains inner-membrane proteins in an α -helical shape. The periplasm contains the peptidoglycan cell wall. The OM is an asymmetric layer, containing PL on the inside and lipopolysaccharide (LPS) on the outside. The OM also contains membrane proteins but in a β -barrel fold. Both membranes contain lipoproteins that are attached to the periplasm side of the membranes (Illustration adapted from Ruiz, Kahne, Silhavy, 2006).

Since half of the OM is built out of LPS, the incorporation of LPS into the OM is essential for bacterial survival and the mechanism is therefore highly conserved. The prevention of LPS in

the OM would be a target of special interest in the development of a new antibiotic drug (Dong *et al.*, 2014).

The LPS transport chain with LptD/E

LPS has three components, Lipid A, core oligosaccharide, and an O-antigen. These components are synthesized and assembled in the cytoplasm and cytoplasmic sides of the IM. Next, LPS is matured at the periplasmic side of the IM. Finally, it is incorporated into the outside of the OM. Therefore, LPS must be transported across the cell envelope from the cytoplasm into the OM (Dong *et al.*, 2014).

This transportation is facilitated by seven LPS transport proteins (LptABCDEFG) which assemble in a complex that spans over the entire cell envelope, with at least one component in every cell envelope department (fig. 12) (Bowyer *et al.*, 2011). The transportation starts with the LptBFG complex, which utilizes energy from ATP-hydrolysis to transport LPS over the IM and transfer it to LptC. The LptC, the soluble periplasmic LptA and the N-terminal domain of LptD form a connection between the inner and outer membrane that allows the transport of LPS over the periplasmic domain. The LPS moves with its Lipid A domain along the hydrophobic groove of this bridge and the energy is provided by ATP-hydrolysis of the LptBFG complex (Botos *et al.*, 2016).

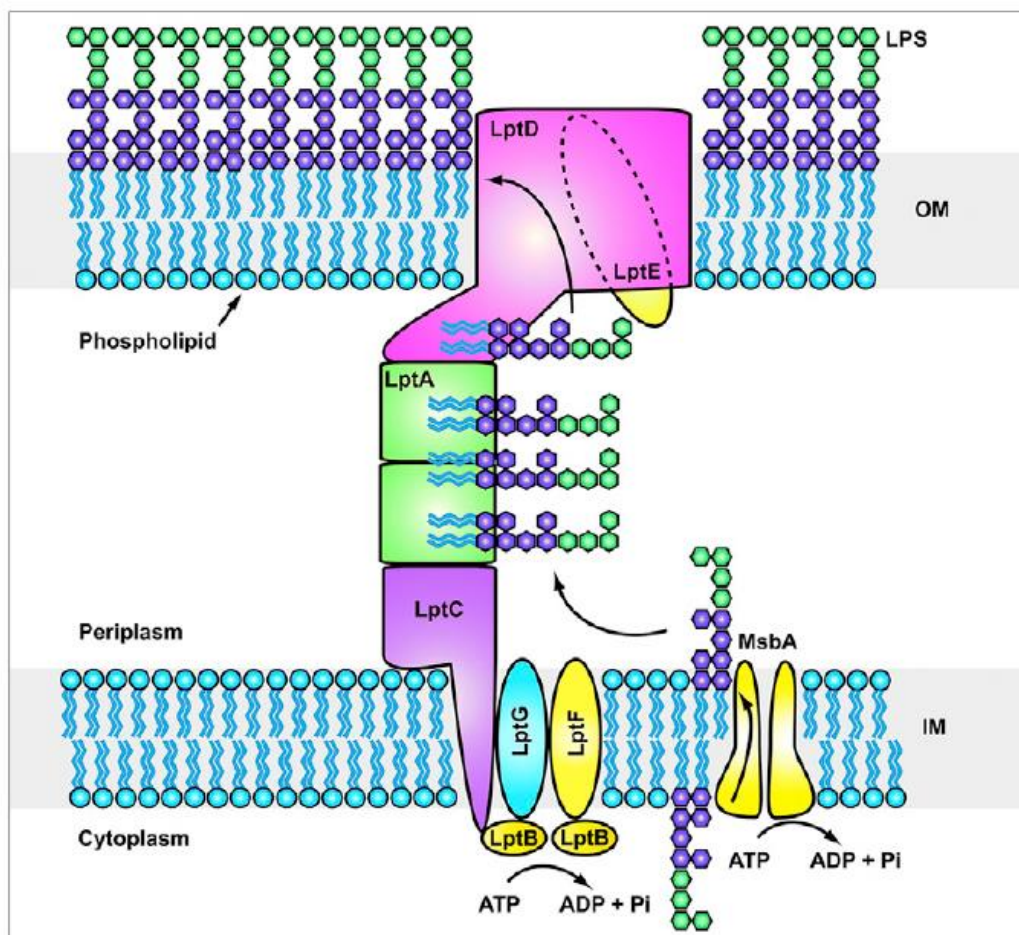


Figure 12. The lipopolysaccharide transport (Lpt) system. The Lpt transport is facilitated by seven proteins (LptABCDEFG). LptBFG transports LPS from the cytoplasm to the inner membrane protein LptC. LPS is further transported across the periplasm by LptA and the N-terminal domain of LptD. The LptD/E complex inserts LPS into the OM (Illustration adapted from Botos *et al.*, 2016).

The final step of transportation is done by the complex of LptD/E, which transports the LPS from the periplasm to the cell surface. LptD is a β -barrel protein and its C-terminal part is integrated into the OM and the N-terminal part has a so-called β -jelly-roll domain. This β -jelly-roll domain connects LptA with LptD. In the lumen of the β -barrel domain is the bound lipoprotein LptE (Andolina *et al.*, 2018). LptE is essential for the folding of LptD which is mediated by the Bam folding machine (Moehle *et al.*, 2016). In different bacterial cells, there are different types of the LptD/E complex. LptD from *Pseudomonas aeruginosa* (*Pa*) has for example an extra insert domain of 100-150 amino acids compared to other LptD's. The function of this insert domain is yet unknown (fig. 13) (Zerbe *et al.*, 2016). The absence of any of the Lpt components will prevent the transportation of LPS to the OM, which would result in the death of the bacteria (Bowyer *et al.*, 2011).

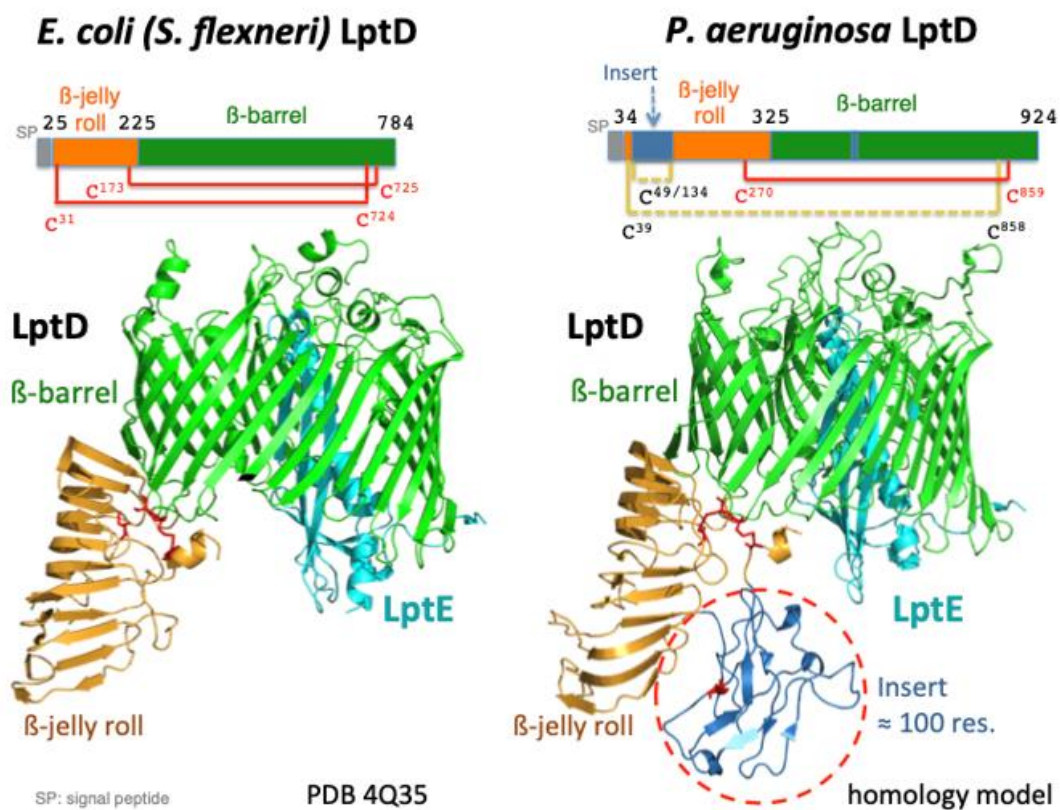


Figure 13. Crystal structures of the LptD/E complex with a β -jelly roll and extra insert in *P. aeruginosa*. LptE (blue) is in the lumen of LptD (green). The β -jelly roll (orange) connects LptD with LptA. *P. aeruginosa* has an extra insert domain (Dark blue) of about 10-150 residues longer than other known LptDs (Illustration adapted from Zerbe *et al.*, 2022)

Murepavadin

Since the transportation of LPS is so highly conserved, it is an interesting target for drug development and since the LptD/E complex is located in the OM, this would be the easiest target. Fortunately, a compound has been discovered which targets the LptD/E complex. This antibiotic is called Murepavadin and is a β -hairpin-shaped peptidomimetic antibiotic (fig. 14). The drug seems to bind the LptD/E complex and inhibits the transportation of LPS to the cell

surface. Nevertheless, Murepavadin is only active at the LptD/E complex of *Pa* which has the extra insert domain (Zerbe *et al.*, 2016).

Pa can cause declining lung function in cystic fibrosis patients and causes high rates of mortality among immune-compromised patients. Since *Pa* is one of the ESKAPE species, it is resistant to most of the available classes of antibiotics. The infections are hard to treat and therefore, a new antibiotic like Murepavadin will have important therapeutic applications (Moehle *et al.*, 2016).

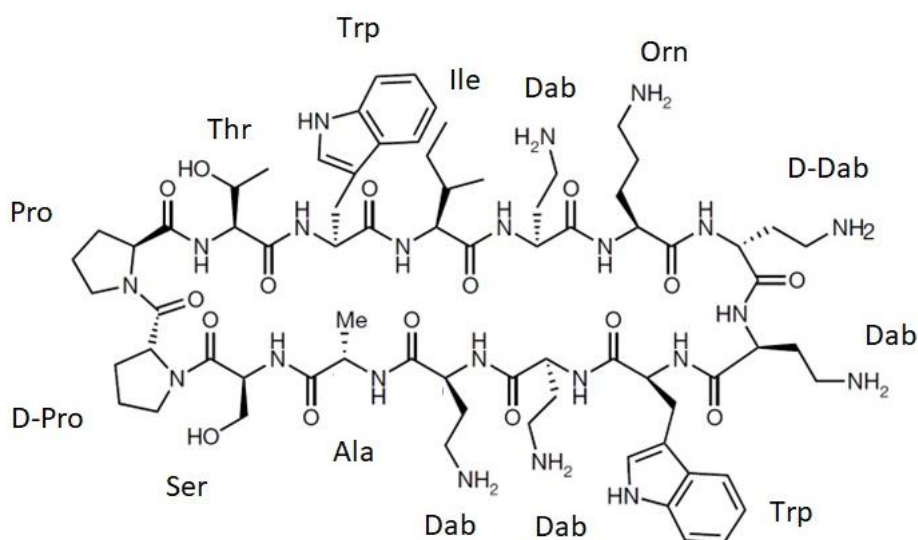


Figure 14. The chemical structure of Murepavadin. Structure of Murepavadin with indicated amino acids. (Illustration adapted from Luther, 2019)

Study objective

A lot of research is done to investigate the working mechanism of this promising drug. Nevertheless, the exact binding location of Murepavadin to LptD/E is unknown. In this study, we aim to find the binding site of Murepavadin to the *Pa* LptD/E β -barrel protein complex by ssNMR and to obtain insight into the bound state of Murepavadin.

Materials and methods

Materials

LptD/E plasmids were obtained from the group of Prof. Dr. John A. Robinson from the University of Zurich.

The modified pET3a vector contained *Pa* LptD, an ampicillin resistance gene and a T7 promoter. The modified pCDFduet-1 vector contained the *Pa* LptE with an N-terminal 6x His-tag, a streptomycin resistance gene, and the T7 promoter.

Transformation of LptD/E_{his}

The two plasmids pET3a and pCDFduet-1 were introduced in *E. coli* BL21 by heat shock. The bacteria were spread out on an LBA plate containing ampicillin and streptomycin (50 mg/ml) and incubated at 37 °C overnight. From the plate, five colonies were selected, streaked out on new plates and grown overnight at 37 °C. Plates were stored at 4 °C.

Miniprep (QLAprep Spin kid) was used to isolate the plasmids and restriction digestion was done at 37 °C for 90 minutes. For LptD restriction enzymes BamH1 and NdeI and the buffer BamHI LSP11091 were used. For LptE restriction enzymes NcoI and XhoI with the buffer R with BSA were used. Gel electrophoresis on 1% agarose gel was run at 80 V for 90 minutes to see if both plasmids and genes were present. After confirming that the plasmids inserts of the correct size were present they were sent for sequencing.

Expression of LptD/E_{his}

The selected colony was grown overnight in a shaking incubator at 37 °C in LB with Ampicillin (25 µg/ml) and Streptomycin (50 µg/ml). At OD₆₀₀= 2.00, the culture was transferred to an unlabelled M9 media and grown overnight at 37 °C. Again, at OD₆₀₀= 2.00, the cells were transferred to a 2-liter ¹⁵N-NH₄Cl labelled M9 media. The media was split into 3 flasks containing 600-700 mL each. The cells were grown for another 4 hours at 37 °C and co-expression of LptD and LptE was induced by the addition of IPTG (100 µM) at OD₆₀₀= 0.6. After cell growth for another 16h at 37 °C, the cells were centrifuged at 4000g for 20 min at 4 °C and resuspended in wash buffer (50 mM PBS (pH 8), 150 mM NaCl, and 25 mM Imidazole (pH 8)). A protease inhibitor and lysozyme were added and the cells were stored at -20 °C.

Purification of LptD/E_{his}

Protocol 1

Cells were thawed on ice. 1 µl of Benzonase, 25 µl MgSO₄ (0.5 mM), and 5 ml PBS (50 mM, Ph 7.4) were added to 50 mL of cells. The cells were put 3 times through a pressure homogenizer. After this, the lysate was centrifuged for 10 min at 10.000g at 4 °C. The supernatant was collected and 2% Tris was added. The cells were left for 30 min and put in the ultra-centrifuge for 1 hour at 48,000 RPM at 4 °C. The pellet was resuspended in buffer (50 mM Tris-HCL pH 7.5, 200 mM NaCl, and 20 mM imidazole) and 1% DDM was added. The resuspended pellet was shaken for 16 hours at 4 °C and after that centrifuged at 370,000g for 60 minutes at 4 °C. The LptD/E_{his} -complex was purified by Ni-affinity chromatography with washing buffer (50

mM PBS pH 8, 150 mM NaCl, 25 mM Imidazole pH8) and Elution buffer (50 mM phosphate buffer pH 8, 150 mM NaCl, 300 mM imidazole, 1% n-octyl- β -D-glucopyranoside (OG)).

Protocol 2

Cells were thawed on ice. 1 μ l of Benzonase, 25 μ l MgSO₄ (0.5 mM), and 5 ml PBS (50 mM, Ph 7.4) were added to 50 mL of culture. The cells were sonicated on ice for 3 x 30s. After this, the lysate was centrifuged for 10 min at 6000g at 4 °C. The supernatant was collected, and the remaining pellet was dissolved in 2 ml of buffer (50 mM PBS, pH 7.4). The pellet was again sonicated for 3x30s and centrifuged for 10 min at 6000g at 4 °C. All the supernatant was put together and diluted with Tris and 0.5% N-Laurosylsarcosine/Ice cold sodium carbonate (0.1 M) and stirred at 4 °C/at room temperature for 1 hour. The mixture was centrifuged at 100,000 g at 4 °C for 1 hour which would give an OM pellet. The OM pellet was washed with Tris (40 mM) and dissolved in PBS (50 mM, pH 7.4) with 1% (w/v) LDAO.

The LptD/E_{his}-complex was purified by Ni-affinity chromatography with washing buffer (50 mM PBS pH 8, 150 mM NaCl, 25 mM Imidazole pH8) and Elution buffer (50 mM phosphate buffer pH 8, 150 mM NaCl, 300 mM imidazole, 1% n-octyl- β -D-glucopyranoside (OG)). A 30 kDa filter was used to separate LptE from the bigger proteins.

Results and Discussion

Transformation of vectors containing LptD and LptE in BL21 cells

We tried to purify the *Pa* LptD/E complex by transforming the plasmids pET3a and pCDFduet-1, containing *Pa* LptD and *Pa* LptE_{his}, respectively into *E. coli* BL21 cells. The transformation was done by heat shock. After the transformation, we used a miniprep to isolate the plasmid DNA. The DNA yield of the plasmids was measured with nanodrop and given in table 2.

Table 2. DNA yield and purity of the plasmids measured by nanodrop.

Culture	ng/ μ L	A260/280	A260/230
LptD	60.5	1.86	1.31
LptE	135.7	1.89	2.00

In the first column, the DNA yield of the plasmids is given in ng/ μ L. The second column gives the ratio of absorbance at 260 nm and 280 nm. This expresses the purity of the DNA. A ratio of 1.8 is accepted as “pure” DNA. The ratio of 260 nm and 230 nm in the third column shows the nucleic acid purity. These values are accepted as “pure” in the range of 2.0-2.2.

After the miniprep, we did restriction digestion to separate the LptD/E genes from the plasmids. This separated DNA was run on gel electrophoresis to see if both LptD/E genes were present in the selected colony. As can be seen in figure 15, there are four bands visible with the right corresponding size for empty vectors and the LptD and LptE genes. Thus confirming that the transformation step worked well and both plasmids were present in the BL21 cells. The isolated plasmids from this colony were sent for sequencing (fig. S4 & S5). The BLAST analysis of this data showed that no considerable mutations occurred and confirm that LptE contains a 6x His-tag (fig. S6 & S7).

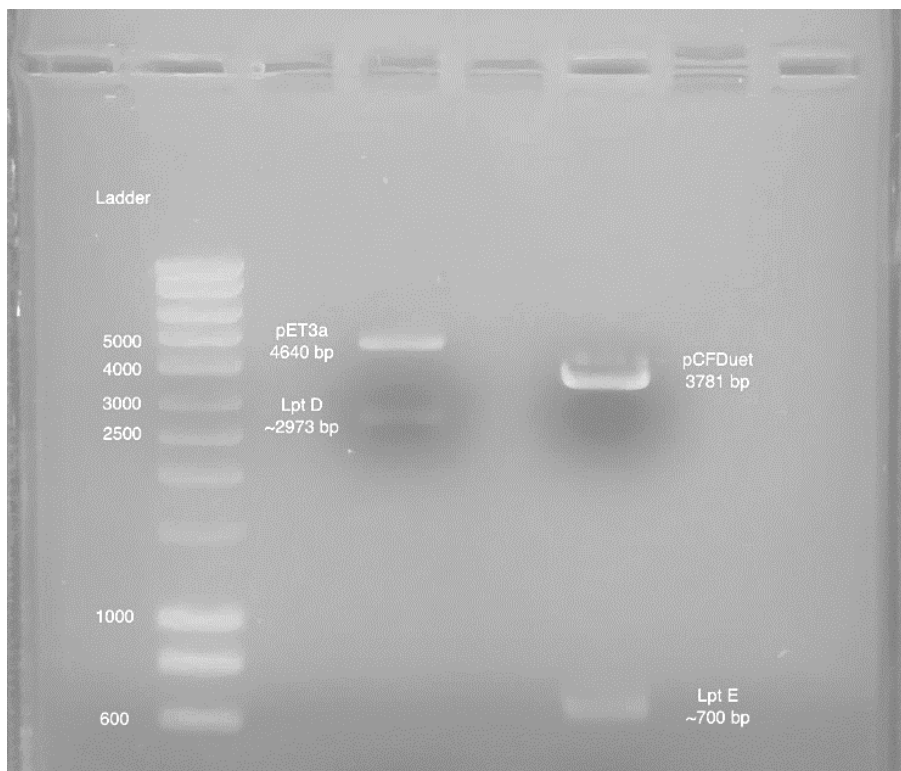


Figure 15. Gel electrophoresis of the restriction digested plasmids. The gel contains four bands, each corresponding to the right size for the two empty vectors and the LptD and LptE genes.

Expression of LptD/E

Since the transformation worked well, we continued with the expression of LptD/E. The T7 promoters of the genes were induced with IPTG. The pre- and post-induced samples were run on an SDS gel to see if there is an increase in expression. As can be seen in figure 16, the indicated bands are darker in the post-induced section at the expected size for LptD and LptE genes. This indicates a higher expression level of LptD/E after the induction.

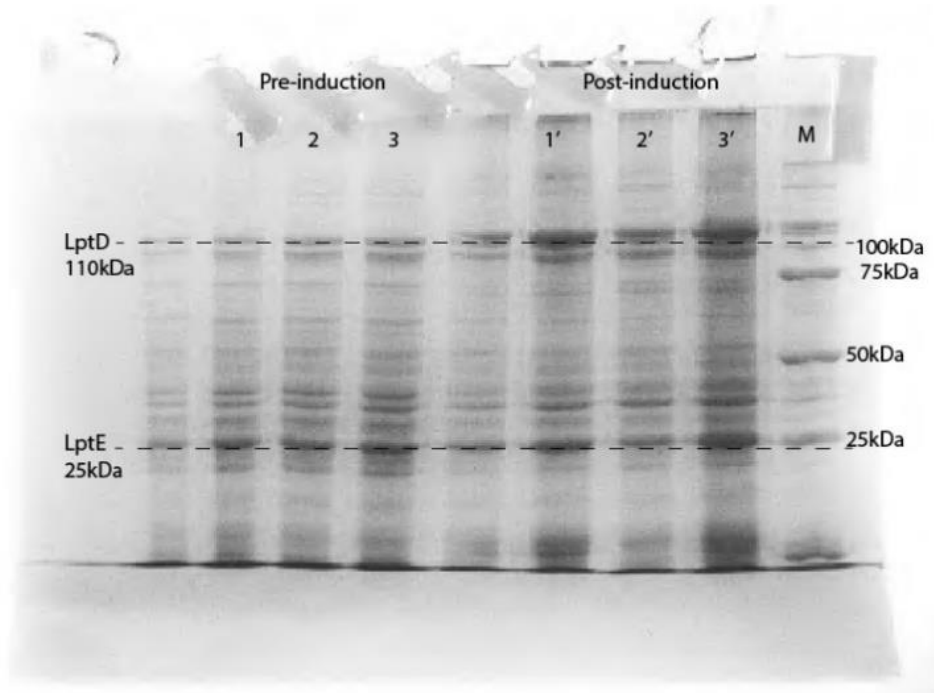


Figure 16. SDS gel with the pre- and post-induced samples. 1, 2 and 3 are pre-induced samples and 1', 2' and 3' are post-induced samples. M is the ladder.

Purification of the LptD/E complex

Since the expression of the LptD/E genes worked well, we continued with the purification of the protein complex. We used two methods as described by Botos *et al.* (2016) and Andolina *et al.* (2018). Unfortunately, the process of purification was more difficult than expected and therefore we did not manage to purify the complex. Here we elaborate on what problems we encountered and what could be addressed in future studies.

First, we tried the method by Botos *et al.* (2016). However, after the first centrifugation step, our proteins were always present in the pellet, whereas in the article, they work with supernatant. One explanation for this problem could be that LptD/E is not very stable and the part that we detect in the pellet is the precipitated LptD/E-complex. There might be very low amounts of LptD/E in the supernatant left that we couldn't detect with SDS gels. Botos *et al.*, also report very low yields of the complex. A solution for this could be to express in larger quantities which would increase the concentrations of LptD/E in the supernatant. Unfortunately, to study the complex using solid-state NMR we would need to produce these in isotopically labelled medium which at such quantities would be very expensive. This could be investigated further in future studies. Maybe more sensitive techniques, like silver-staining SDS, can show whether the complex is still present in the supernatant.

Furthermore, we also tried different detergents to extract the LptD/E-complex out of the pellet. Instead of the 1% DDM, we tried 5% Brij-58, 2% DM, and 5% Triton. These detergents

were still unable to extract the complex as we could detect high amounts of LptD and LptE in the pellet (fig. S8).

Secondly, we followed the method of Andolina *et al.* (2018). This time we were only able to purify LptE (fig. S9). This indicates that LptE was not strongly associated in a bound complex with LptD. Since LptD does not contain a His-tag, it could only be purified by Nickel-affinity if it strongly binds to LptE. A possible solution for this could be to put a His-tag on the LptD gene as well. This is also done in the study by Botos *et al.* and does not influence the complex folding. Another option is to put LptD and LptE in the same vector. This might enhance the complex formation. Finally, the purified LptE also showed instability during storage at 4 °C over a period of a few weeks (fig. S10). It should be used as soon as it is purified or else it precipitates. The complex of LptD/E might precipitate even faster.

In conclusion, in this study, we wanted to investigate the binding mechanism of Murepavadin to the *Pa.* LptD/E complex. Unfortunately, we did not manage to purify LptD/E. Therefore, we give insight into the problems encountered and the troubleshooting approach for the purification steps of the LptD/E complex. We concluded that there might be very low amounts of usable LptD/E in the cell lysate and most of it is precipitated. We were not able to detect this with the SDS gel. Furthermore, after following a different protocol we were only able to purify LptE with Ni-affinity. But LptE is also very unstable and precipitated within a few days after purification. Finally, we didn't find any detergents that would help with the purification of the complex from the pellet.

Further efforts are required to optimize the purification protocol before the binding mechanism of Murepavadin can be established. Further steps can include the usage of one plasmid with both LptD and LptE genes, the addition of a His-tag on LptD as well, expressing in larger quantities to increase the LptD/E concentration, or the use of other detergents.

Acknowledgments

Hereby, I would like to thank Dr. Markus Weingarth for providing me with this internship and the all the helpful discussions. I would also like to thank Rhythm Shukla for her excellent supervision, explanations, and meaningful discussions as a daily supervisor. Moreover, I would like to thank Maik Derks, Raj Kumar, Raymond Schellevis, and Roy van Beekveld for their help, explanations, and ideas for different experiments. Finally, I would like to thank the entire NMR department for having me and for creating a nice working environment.

Supplementary Data

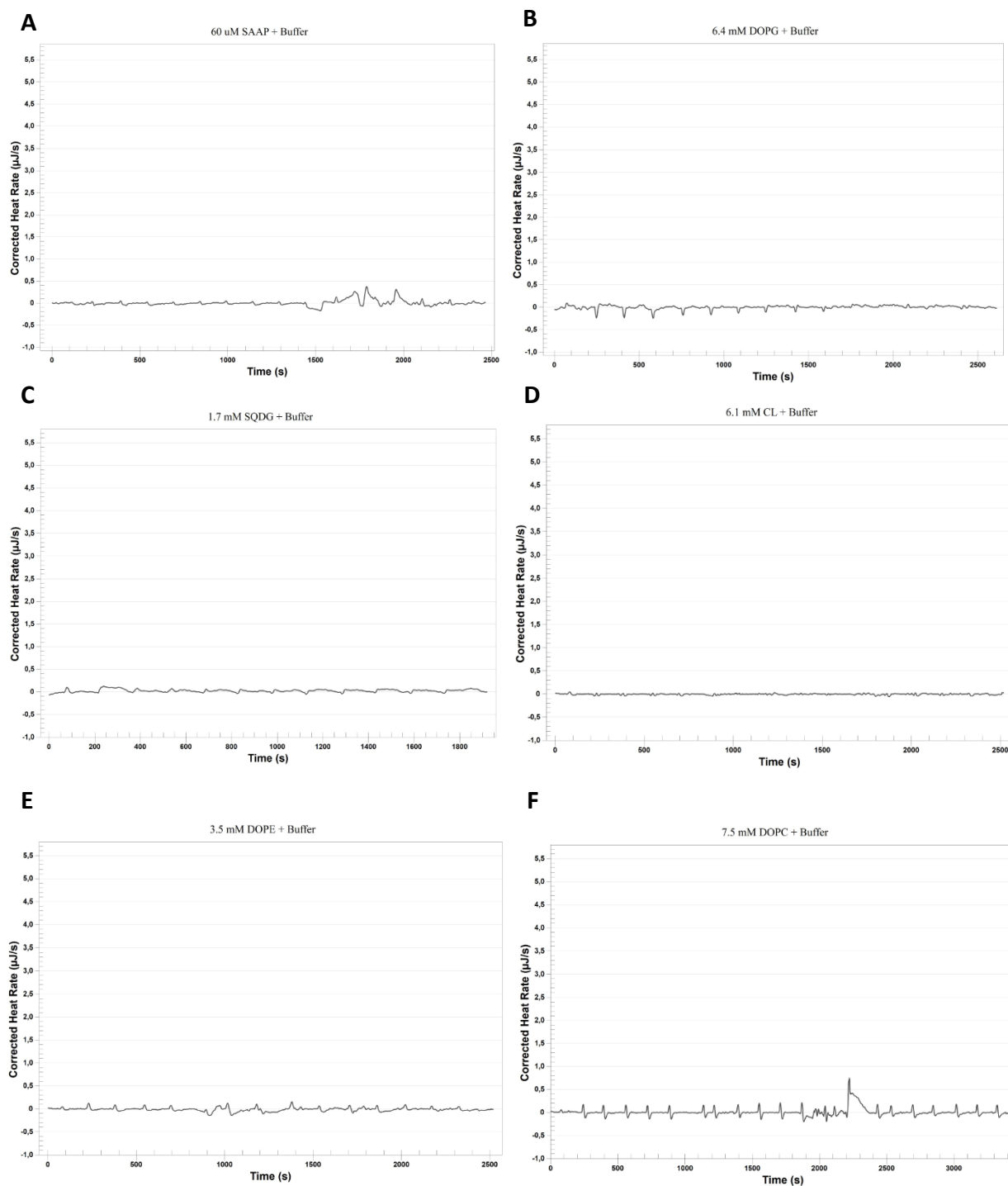


Figure S1. ITC buffer titrations for different lipids. A) SAAP-148, B) DOPG, C) SQDG, D) Cardiolipin, E) DOPC, F) DOPE.

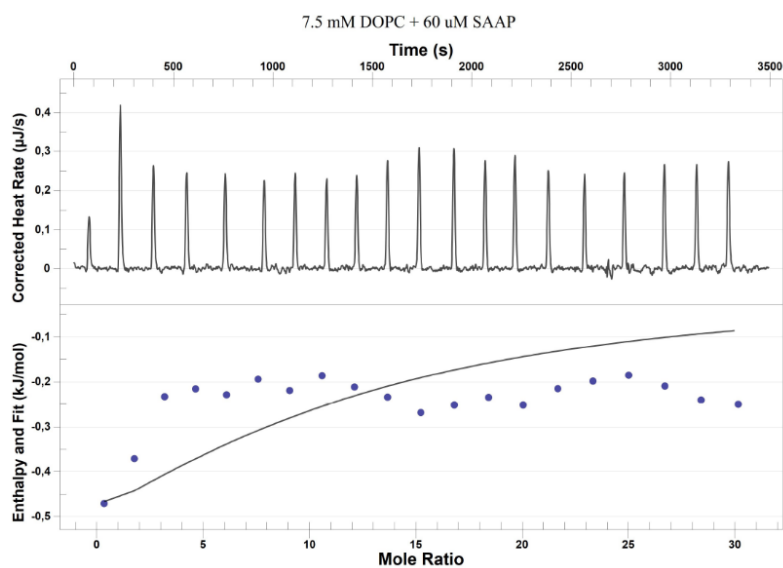


Figure S2. Zoom-in of DOPC thermogram. The zoom-in of figure 8D.

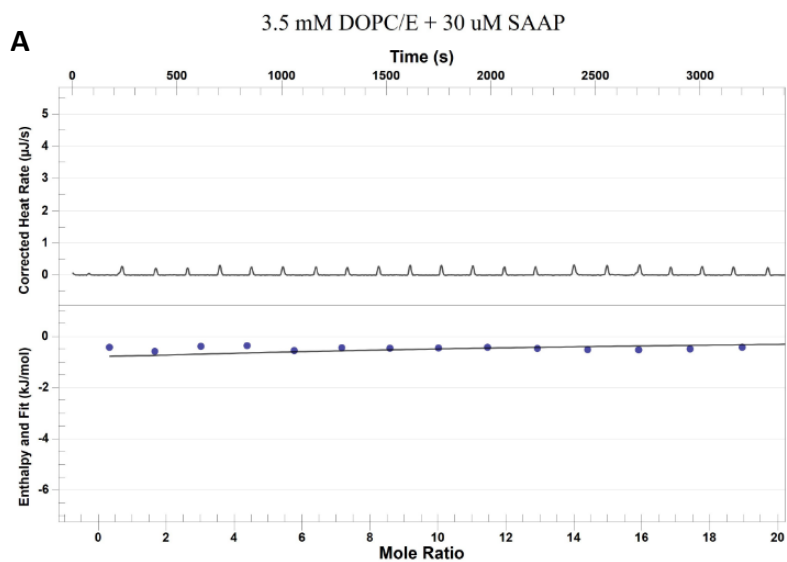


Figure S3. ITC data of DOPE LUVs with SAAP-148. (A) The top panel shows the corrected heat release whereby every peak corresponds with an injection. The line in the lower panel indicates the best fit with the independent model. Experiments were performed in duplicates. Mean best fit values with SD: $K_D = 1,00\text{E-}03 \pm 0 \text{ M}$ (B) zoomed-in version of thermogram A.

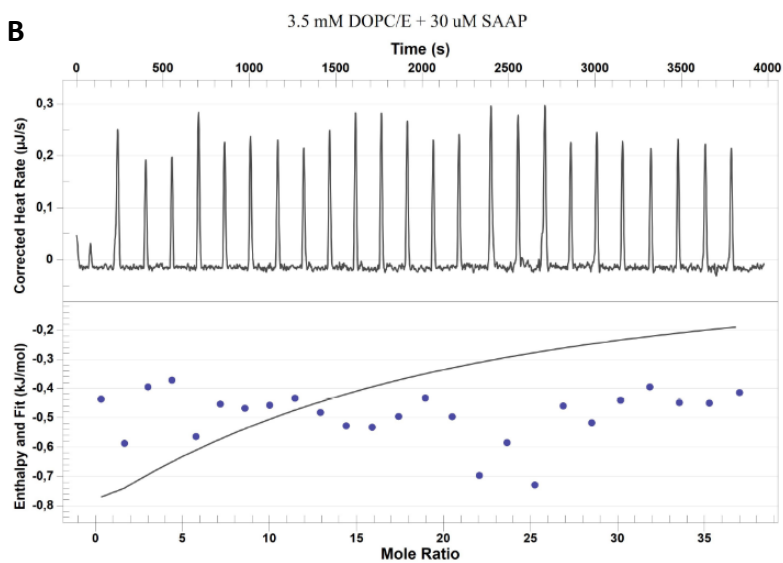




Figure S4. The sequencing results of LptE. Sequencing of the LptE plasmid performed by MacroGen.



Figure S5. The sequencing results of LptD. Sequencing of the LptD plasmid performed by MacroGen.

>LPS assembly lipoprotein LptE [Pseudomonas aeruginosa]
 Sequence ID: WP_152372638.1 Length: 207
 Range 1: 2 to 207

Score:343 bits(881), Expect:2e-113,
 Method:Compositional matrix adjust.,
 Identities:203/206(99%), Positives:204/206(99%), Gaps:0/206(0%)

```

Query 69  KRILTSAALIGMTLLAACGFQLRGLGDAQFALKEIDVSARNAYGPTVRELKETLENSGV 248
          KRILTSAALIGMTLLAACGFQLRGLGDAQFALKEIDVSARNAYGPTVRELKETLENSGV
Sbjct 2   KRILTSAALIGMTLLAACGFQLRGLGDAQFALKEIDVSARNAYGPTVRELKETLENSGV 61

Query 249 KVTSNAPYHLVLVREDNQQRVTSYTGSAARGAEFELTNTINYEIVGANDLVLMNSQVQVQK 428
          KVTSNAPYHLVLVREDNQQRVTSYTGSAARGAEFELTNTINYEIVGANDLVLMNSQVQVQK
Sbjct 62  KVTSNAPYHLVLVREDNQQRVTSYTGSAARGAEFELTNTINYEIVGANDLVLMNSQVQVQK 121

Query 429  VYVHDENNLIGSDQEAALRSEMRRDLIQQLSMRLQALTPAQLDeaqrqa*akakaeaea 608
          VYVHDENNLIGSDQEAALRSEMRRDLIQQLSMRLQALTPAQLDEAQRQA AKAK+EAEA
Sbjct 122 VYVHDENNLIGSDQEAALRSEMRRDLIQQLSMRLQALTPAQLDEAQRQAEAKAKSEAEA 181

Query 609  lraadeaerqrraaepqqSPIEFPTP 686
          LRAADEA RQRRAAEPQQSPIEFPTP
Sbjct 182  LRAADEAGRQRRAAEPQQSPIEFPTP 207
  
```

Figure S6. BLAST alignment of LptE.

Sequence ID: QDR43257.1 Length: 468
 Range 1: 1 to 403

Score:662 bits(1707), Expect:0.0,
 Method:Compositional matrix adjust.,
 Identities:356/403(88%), Positives:364/403(90%), Gaps:3/403(0%)

```

Query 53  MAVKSLVFRRKFP LLVTGSL LALQPVAALTVQAADQFDCKVSATGGWDCSPLQANANL P 232
          MAVKSLVFRRKFP LLVTGSL LALQPVAALTVQAADQFDCKVSATGGWDCSPLQANANL P
Sbjct 1   MAVKSLVFRRKFP LLVTGSL LALQPVAALTVQAADQFDCKVSATGGWDCSPLQANANL P 60

Query 233 PRPAHTatsvstaaagssvsgsggetveaePTQRLVTESGGRALKRSADYSHLDWIPRE 412
          PRPAHTATS VSTAAAG+SVSGSGGETVEAEPTQRLVTESGGRALKRSADYSHLDWIPRE
Sbjct 61  PRPAHTATS VSTAAAGTSVSGSGGETVEAEPTQRLVTESGGRALKRSADYSHLDWIPRE 120

Query 413  KLTAQAQLAEIGPYCGGSYIEPVRPGMDDGAPSDSPTYVSAKASRYEQEKQIATLAGDVV 592
          KLTAQAQLAEIGPYCGGSYIEPVRPGMDDGAPSDSPTYVSAKASRYEQEKQIATLAGDVV
Sbjct 121  KLTAQAQLAEIGPYCGGSYIEPVRPGMDDGAPSDSPTYVSAKASRYEQEKQIATLAGDVV 180

Query 593  LRQGS MQVEGDEANLHQLENRGELVGNVKLRDKGMLVVG DHAQVQLDNGEAQVDNAEYVI 772
          LRQGS MQVEGDEANLHQLENRGELVGNVKLRDKGMLVVG DHAQVQLDNGEAQVDNAEYVI
Sbjct 181  LRQGS MQVEGDEANLHQLENRGELVGNVKLRDKGMLVVG DHAQVQLDNGEAQVDNAEYVI 240

Query 773  HKAHARGSALYAKRSENAIIMLKDGT YRCEPSSNAWTLKGN NVKLN PATGFGTATNATL 952
          HKAHARGSALYAKRSENAIIMLKDGT YRCEPSSNAWTLKGN NVKLN PATGFGTATNATL
Sbjct 241  HKAHARGSALYAKRSENAIIMLKDGT YRCEPSSNAWTLKGN NVKLN PATGFGTATNATL 300

Query 953  RVKDFPVFYTPYIYFPIDRRRQSGFLPPSFSSTAKPGLPWV -PRTTSTGANYNPRCTPPN 1129
          RVKDFPVFYTPYIYFPIDRRRQSGFLPPSFSST+ G V P + NY+ P
Sbjct 301  RVKDFPVFYTPYIYFPIDRRRQSGFLPPSFSSTSDTGFTLVTPYYFNLPNYDATLYPRY 360

Query 1130 -GQRGLMLEGEFRSLTPKKERFFTLPLK -KEKTPQKFP GK K 1252
          +RG+MLEGEFR LT E T L K+ + FP K
Sbjct 361  MAKRGMMLEGEFRYLTHSSEGMVTAAYLNDKDDHRENFDPYSK 403
  
```

Figure S7. BLAST alignment of LptD.

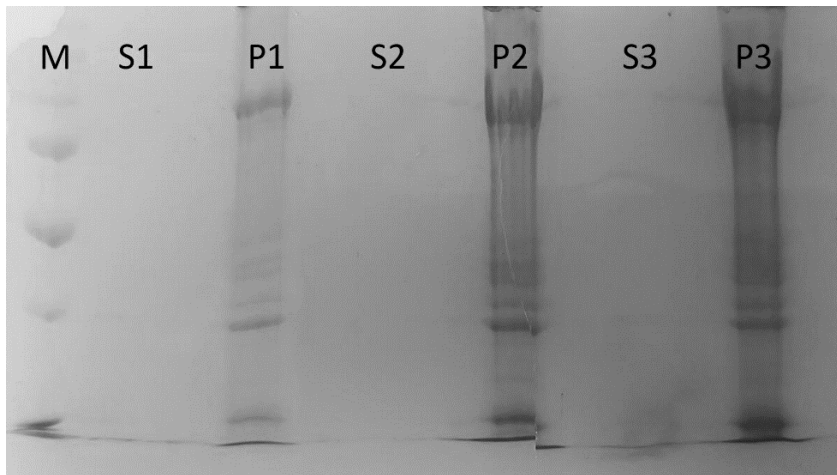


Figure S8. SDS gel of the supernatant and pellet with the different detergents. M is the ladder. S1 and P1 stand for the supernatant and pellet of 5% Triton, S2 and P2 stand for 5% Brij58 and S3 and P3 stand for the 2% DDM.

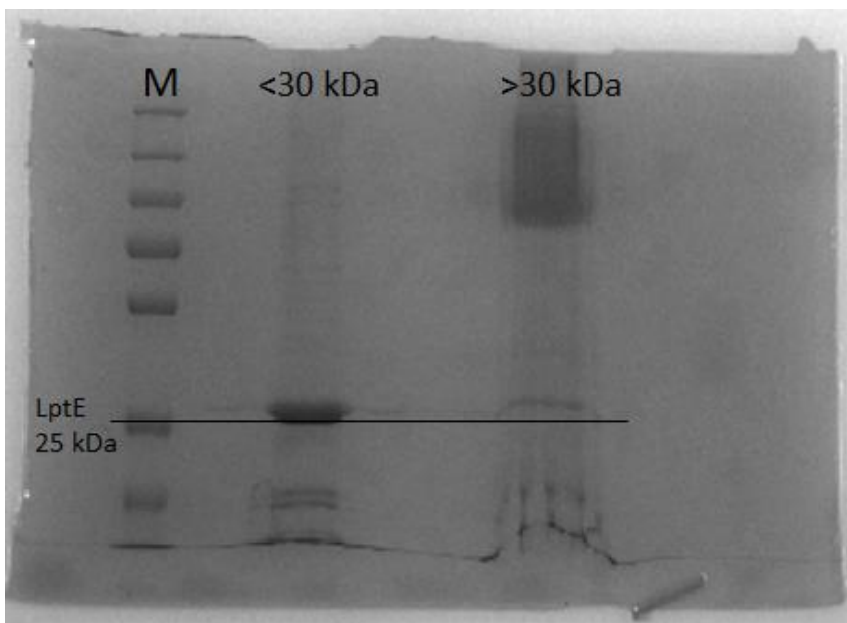


Figure S9. SDS gel after the use of a 30 kDa filter for LptE purification. M is the ladder, in the second column are the proteins that came through the filter of 30 kDa, and in the final column are the proteins that stayed on top of the filter and thus are bigger than 30 kDa. The LptE is visible in the <30 kDa column.

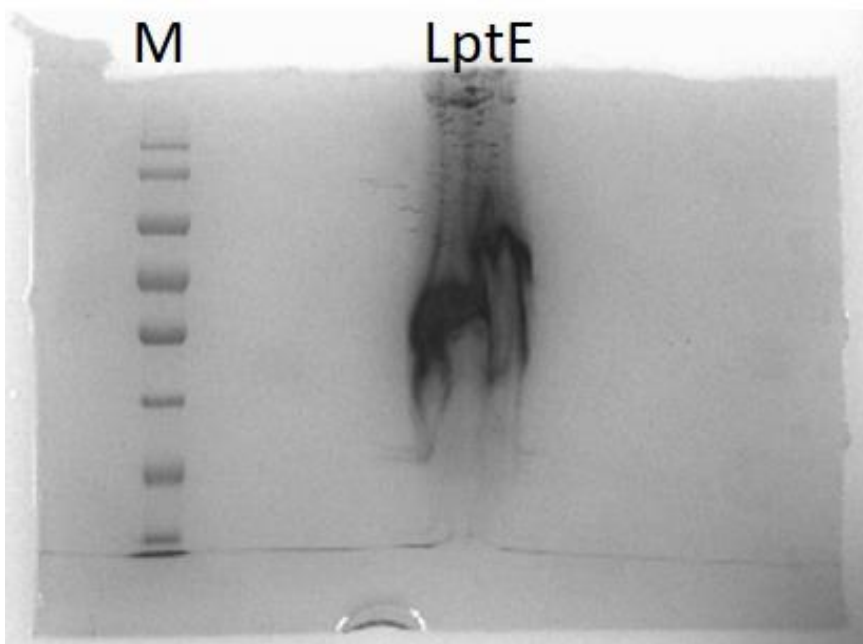


Figure S10. SDS gel of purified LptE after 3 weeks. M is the ladder and in the second column was the LptE sample.